

¹ **GLO-Roots: an imaging platform enabling multidimensional characterization of soil-grown roots systems**

³ Rubén Rellán-Álvarez^{1, 9}, Guillaume Lobet², Heike Lindner^{1, 8}, Pierre-Luc Pradier^{1, 8, 10},
⁴ Jose Sebastian^{1, 8}, Muh-Ching Yee¹, Yu Geng^{1, 7}, Charlotte Trontin¹, Therese LaRue³,
⁵ Amanda Schrager-Lavelle⁴, Cara H. Haney⁵, Rita Nieu⁶, Julin Maloof⁴, John P. Vogel⁷,
⁶ José R. Dinneny^{1, 12}

⁷ ¹ Department of Plant Biology, Carnegie Institution for Science, Stanford, CA, USA.

⁸ ² PhytoSystems, University of Liège, Liège, Belgium.

⁹ ³ Department of Biology, Stanford University, Stanford, CA, USA.

¹⁰ ⁴ Department of Plant Biology, UC Davis, Davis, CA, USA.

¹¹ ⁵ Harvard Medical School/Massachusetts General Hospital, Department of Genetics/¹² Department of Molecular Biology Boston, MA, USA

¹³ ⁶ USDA Western Regional Research Center, Albany, CA, USA

¹⁴ ⁷ DOE Joint Genome Institute, Walnut Creek, CA, USA

¹⁵ ⁸ These authors contributed equally

¹⁶ ⁹ Present address: Laboratorio Nacional de Genómica para la Biodiversidad (Langebio),
¹⁷ Unidad de Genómica Avanzada, Centro de Investigación y de Estudios Avanzados del Insti-
¹⁸ tuto Politécnico Nacional (CINVESTAV-IPN), Irapuato, Guanajuato, México

¹⁹ ¹⁰ Present address: Boyce Thompson Institute for Plant Research/USDA, Ithaca, NY, USA.

²⁰ ¹¹ Present address: Energy Biosciences Institute, UC, Berkeley, CA, USA

²¹ ¹² Corresponding author

²² **Author contributions:**

²³ RR-A: Conception, design and development of the growth and imaging system and Arabidop-
²⁴ sis transgenic lines; acquisition, analysis and interpretation of data; drafting and revising

25 the article.

26 GL: Development of the GLO-RIA image analysis plugin, analysis and interpretation of

27 data, drafting and revising the article.

28 HL: Acquisition of data, development of the tomato growth and imaging setup.

29 P-LP: Acquisition of data, analysis and interpretation of data

30 JS: Development of Brachypodium transgenic lines, acquisition and analysis of Brachy-

31 podium, Arabidopsis and tomato data.

32 MCY: Development of Arabidopsis and Brachypodium transgenic lines.

33 YG: Development of Arabidopsis transgenic lines.

34 CT: Acquisition and analysis of the QPCR data

35 TL: Acquisition and analysis of the QPCR data

36 AS-L: Contributed the unpublished dual-color tomato line.

37 CH: Contributed the unpublished *Pseudomonas fluorescens* CH267-lux strain.

38 RN: Contribution to the development of the Brachypodium transgenic line.

39 JM: Contributed the unpublished dual-color tomato line.

40 JPV: Contribution to the development of the Brachypodium transgenic line.

41 JRD: Conception, design and development of the growth and imaging system and Arabidop-

42 sis transgenic lines; acquisition, analysis and interpretation of data; drafting and revising

43 the article.

44 All authors read and approve the final version of the manuscript.

45 **Abstract**

46 Root systems develop different root types that individually sense cues from their local envi-

47 ronment and integrate them with systemic signals. This complex multi-dimensional amal-

48 gam of inputs leads to continuous adjustment of root growth rates, direction and metabolic

49 activity to define a dynamic physical network. Current methods for analyzing root biology
50 balance physiological relevance with imaging capability. To bridge this divide, we devel-
51 oped an integrated imaging system called Growth and Luminescence Observatory for Roots
52 (GLO-Roots) that uses luminescence-based reporters to enable studies of root architecture
53 and gene expression patterns in soil-grown, light-shielded roots. We have developed image
54 analysis algorithms that allow the spatial integration of soil properties such as soil moisture
55 with root traits. We propose GLO-Roots as a system that has great utility in both present-
56 ing environmental stimuli to roots in ways that evoke natural adaptive responses, and in
57 providing tools for developing a multi-dimensional understanding of such processes.

58 Introduction

59 Plant roots are three-dimensional assemblies of cells that coordinately monitor and acclimate
60 to soil environmental change by altering physiological and developmental processes through
61 cell-type and organ-specific regulatory mechanisms^{1,2}. Soil comprises a complex distribution
62 of particles of different size, composition and physical properties, airspaces, variation in
63 nutrient availability and microbial diversity^{3,4}. These physical, chemical and biological
64 properties of soil can vary on spatial scales of meters to microns, and on temporal scales
65 ranging from seasonal change to seconds. Root tips likely monitor this environment through
66 locally and systemically acting sensory mechanisms^{5,6}.

67 The architecture of the root system determines the volume of soil where resources can be
68 accessed by the plant (rhizosphere) and is under both environmental and genetic control.
69 Plasticity in growth parameters allows the plant to adjust its form to suit a particular soil.
70 Lateral roots, which usually make up the majority of the total root system, often grow at an
71 angle divergent from the gravity vector. This gravity set-point angle (GSA) is controlled by
72 auxin biosynthesis and signaling and can be regulated by developmental age and root type⁷.
73 Recent cloning of the *DRO1* Quantitative Trait Locus (QTL) demonstrates that natural
74 genetic variation is a powerful tool for uncovering such control mechanisms⁸.

75 Specific root ideotypes (idealized phenotypes) have been proposed to be optimal for acquisi-

76 tion of water and nitrogen, which are distinct from ideotypes for low phosphorus. Based on
77 computational modeling and field studies, the “steep, deep and cheap” ideotype proposed by
78 Lynch and colleagues may provide advantages to the plant for capturing water and elements
79 like nitrogen that are water soluble and therefore tend to move in the soil column with water.
80 This ideotype consists of highly gravitropic, vertically oriented roots that grow deep in the
81 soil column and develop large amounts of aerenchyma, which reduces the overall metabolic
82 cost of the root system³. Other elements, like phosphorus that are not water soluble and
83 are tightly bound to organic matter usually accumulate in the top layers of soil favor roots
84 systems that are more highly branched and shallow effectively increasing the effective root
85 exploration surface in the top layers of soil³. Modeling of root system variables shows that
86 optimum architecture for nitrogen and phosphorus uptake are not the same⁹ and suggests
87 tradeoffs that may affect the evolution of root architecture as a population adapts to a
88 particular environmental niche.

89 Clearly, understanding the architecture of root systems and how environmental conditions
90 alter root developmental programs is important for understanding adaptive mechanisms
91 of plants and for identifying the molecular-genetic basis for different response programs. In
92 addition, root systems have complexity beyond their architecture that needs to be incorpo-
93 rated into our understanding of plant-environment interactions. Primary and lateral roots
94 exhibit different stress response programs in *Arabidopsis*² and may play specialized roles
95 in water and nutrient uptake. Thus, it is important to develop methods that allow for a
96 multidimensional characterization of the root system that includes growth, signaling, and
97 interactions with other organisms. Furthermore, physiological parameters that affect whole
98 plant responses to the environment, such as transpiration, are likely integrated into such
99 processes, thus requiring a more holistic approach to studies of root function.

100 Based on these considerations we have developed a new root imaging platform, Growth
101 and Luminescence Observatory for Roots (GLO-Roots), which allows root architecture and
102 gene expression to be studied in soil-grown plants. GLO-Roots is an integrated system
103 composed of custom growth vessels, luminescent reporters and imaging systems. We use

104 rhizotrons that have soil volumes equivalent to small pots and support growth of Arabidopsis
105 from germination to senescence. To visualize roots, we designed plant-codon optimized
106 luciferase reporters that emit light of different wavelengths. To visualize reporter expression,
107 plants are watered with a dilute luciferin solution and imaged afterwards. We have built
108 a custom luminescence imaging system that automatically captures images of rhizotrons
109 held vertically. The signal from each reporter is distinguished using band-pass filters held
110 in a motorized filter wheel, which enables automated acquisition of images from plants
111 expressing both structural and environmentally and developmentally responsive reporters.
112 We have also developed GLO-RIA (GLO-Roots Image Analysis), an ImageJ¹⁰ plugin that
113 allows for automated determination of root system area, convex hull, depth, width and
114 directionality, which quantifies the angle of root segments with respect to gravity. GLO-
115 RIA is also able to relate root system parameters to local root-associated variables such as
116 reporter expression intensity or soil-moisture content.

117 Overall GLO-Roots has great utility in presenting environmental stimuli to roots in phys-
118 iologically relevant ways and provides tools for characterizing responses to such stimuli at
119 the molecular level of whole adult root systems over broad time scales.

120 **Box 1.**

121 All resources for GLO-Roots, including the user manual, the latest software downloads, the
122 source code, the original raw data used in the manuscript and sample images can be found
123 on https://github.com/rr-lab/glo_roots.

124 **Results**

125 We have developed an integrated platform for growing, imaging and analyzing root growth
126 that provides advances in physiological relevance and retains the ability to visualize aspects
127 of root biology beyond structure.

¹²⁸ **The GLO-Roots plattform**

¹²⁹ GLO-Roots is comprised of four parts: i) growth vessels called rhizotrons that allow plant
¹³⁰ growth in soil and root imaging; ii) luminescent reporters that allow various aspects of
¹³¹ root biology to be tracked in living plants; iii) luminescence imaging system designed to
¹³² automatically image rhizotrons; iv) GLO-RIA, an image analysis suite designed to quantify
¹³³ root systems imaged using GLO-Roots.

¹³⁴ **Plant growth system** GLO-Roots utilizes custom designed growth vessels classically
¹³⁵ known as rhizotrons, which hold a thin volume of soil between two sheets of polycarbonate
¹³⁶ plastic. Acrylic spacers provide a 2-mm space in which standard peat-based potting mix
¹³⁷ is added. Black vinyl sheets protect roots from light and rubber U-channels clamp the
¹³⁸ rhizotron materials together. Plastic racks hold the rhizotrons vertically and further protect
¹³⁹ the roots from light. Rhizotrons and rack are placed in a black tub and water are added, to
¹⁴⁰ a depth of about 2 cm, at the bottom to maintain moisture in the rhizotrons during plant
¹⁴¹ growth. The volume of soil in the rhizotrons (100 cm^3) is similar to small pots commonly
¹⁴² used for Arabidopsis and supports growth throughout the entire life cycle (Fig 1A-C and
¹⁴³ Supplement 1).

¹⁴⁴ To determine how the biology of plants grown in rhizotrons compares to other standard
¹⁴⁵ growth systems, we utilized high-throughput qRT-PCR to study how these conditions af-
¹⁴⁶ fect expression of 77 marker genes in root and shoot samples. These genes were curated
¹⁴⁷ from the literature and belong to a wide array of biological pathways including nutrient
¹⁴⁸ acquisition, hormone and light response and abiotic stress. Whole roots and shoot samples
¹⁴⁹ were collected at the end of the light and dark cycles (16 hour light, 8 hours dark) from
¹⁵⁰ plants grown in rhizotrons, pots, and petri dishes with two different media compositions (1X
¹⁵¹ Murashige and Skoog basal salts (MS), 1% sucrose or 0.25X MS, no sucrose). Principal com-
¹⁵² ponent analysis of the gene expression values showed a separation of soil and gel-grown root
¹⁵³ systems in the the first principal components (Figure 1-figure supplement 1A). We observed
¹⁵⁴ enhanced expression of genes associated with light-regulated pathways (flavonoid biosynthe-

sis: *FLAVINOL SYNTHASE1*, *FLS1*, *CHALCONE SYNTHASE*, *CHS*), (photosynthesis: *RUBSICO SUBUNITS1A*, *RBCS1A CYCLOPHILIN 38*, *CYP38*), which is expected due to the exposure of gel-grown roots to light. In addition, genes associated with phosphorus nutrition (*LOW PHOSPHATE RESPONSE1*, *LPR1*, *PHOSPHATE STARVATION RESPONSE1*, *PHR1*) were among others (Figure 1-figure table supplement 1) expressed predominantly in soil-grown roots, suggesting differences in nutrient availability between the different growth systems Interestingly, shoot samples where not clearly distinguished by growth media and, instead, time of day had a greater effect (Figure 1-Supplement 2). These data suggest root systems may be particularly sensitive to media conditions and indicate that rhizotron-grown root systems more closely approximate the biology of a pot-grown plant than standard gel-based media. Shoot weight and primary root length were significantly reduced for gel-grown plants compared to rhizotron- or pot-grown plants suggesting significant differences in the biology of plants grown under these conditions (Figure 1-figure supplement 1B-C). While the 2 mm depth of the soil sheet is 10 to 20 times the average diameter of an Arabidopsis root (between 100-200 microns), we evaluated whether rhizotron-grown plants exhibited any obvious stress as a consequence of physical constriction. We compared traits of plants growing in vessels that hold similar volumes of soil but in different volumetric shapes. The number of lateral roots was significantly lower in pot and cylinder-grown plants compared to rhizotron-grown plants (Figure 1-figure supplement 1D) whereas primary root length of rhizotron and cylinder-grown plants was significantly greater than pot-grown plants (Figure 1-figure supplement 1E). No significant differences in shoot area were observed between the three systems (Figure 1-figure supplement 1-data). Thus, these data do not support the hypothesis that rhizotron-grown plants experience physical constriction greater than other vessels holding the same volume of soil.

Generation of transgenic plants expressing different luciferases Arabidopsis roots cannot easily be distinguished from soil using brightfield imaging due to their thinness and translucency (Figure 1-figure supplement 3); thus, reporter genes are needed to enhance the contrast between the root and their environment. Luciferase is an ideal reporter to visualize

roots: 1) unlike fluorescent reporters, luciferase does not require high-intensity excitation light, which could influence root growth, 2) peat-based soil (a type of histosol) exhibits no autoluminescence but does autofluoresce at certain excitation wavelengths similar to GFP (Figure 1-figure supplement 3), 3) while GFP is very stable, and thus not as suitable for imaging dynamic transcriptional events, the luciferase enzyme is inactivated after catabolism of luciferin, making it ideal for studying processes such as environmental responses. A considerable number of luciferases have been developed that emit light spanning different regions of the visible spectrum, but their utilization has been limited to studies in animals (Table 1).

To determine the efficacy of using luciferase to visualize roots in soil, we codon optimized sequences of *PpyRE8*, *CBGRed*, *LUC2*, and *CBG99* for Arabidopsis expression. In addition, nanoLUC and venus-LUC²¹ were utilized. Constitutive luciferase expression was driven in plants using the *UBIQUITIN 10* (*UBQ10*) or *ACTIN2* (*ACT2*) promoter using vectors assembled through a Golden-Gate cloning system¹². Plants homozygous for a single locus T-DNA insertion were evaluated for in vivo emission spectra and luminescence intensity (Fig 1D). All the evaluated luciferases use D-luciferin as a substrate facilitating the simultaneous imaging of different luciferases except nanoLUC, which uses a proprietary substrate furimazine. In general, luciferases with red-shifted emission spectra were less intense than the green-shifted luciferases (Fig 1D). LUC2o showed an emission maximum at 580 nm and a minor peak at 620 nm while CBG99o lacks the minor peak.

GLO1: a semi-automated luminescence imaging system for rhizotrons Luminescence imaging systems commercially available for biomedical research are usually optimized for imaging horizontally held specimens or samples in microtiter plates. Placing rhizotrons in this position would induce a gravitropic response in plants. Working with Bioimaging Solutions (San Diego, CA) we designed and built a luminescence imaging system optimized for rhizotron-grown plants. GLO1 (Growth and Luminescence Observatory 1) uses two back-thinned CCD cameras (Princeton Instruments, USA) to capture partially-overlapping images of rhizotrons while a motorized stage automatically rotates the rhizotron to capture

211 images of both sides (Fig 1E). A composite image is generated from the images of each side;
212 Fig 1F shows that approximately half of the root system is revealed on each side with few
213 roots being visible on both sides. Apparently, the soil sheet is thick enough to block portions
214 of the root system but thin enough to ensure its continuous structure can be compiled from
215 opposite face views. We tested the ability of GLO1-generated images to reveal complete
216 root systems by manually quantifying the number of lateral roots in excavated root systems
217 of 8 different plants and testing these results against estimates of lateral root number from
218 images of the same plants visually inspected by 4 different persons. These comparisons
219 revealed good correlation ($(R^2 = 0.974)$) between actual lateral root counts and image-based
220 estimation, indicating GLO1-generated root images provide an accurate representation of
221 the in soil root system.

222 Continuous addition of luciferin did not have any significant effect on shoot weight or primary
223 root length (Figure 1-figure supplement 4). After luciferin addition, luminescence signal
224 could be reliably detected in root systems for up to 10 days, depending on the developmental
225 state of the plant.

226 **GLO-RIA: GLO-Roots Image Analysis** We developed a set of image analysis algo-
227 rithms that were well suited for the complex root systems that GLO-Roots is able to capture.
228 GLO-RIA (Growth and Luminescence Observatory Root Image Analysis) is an ImageJ plu-
229 gin divided in two modules. The first module (RootSystem) performs four different types of
230 analysis: i) a local analysis that detects all root particles in the image and computes their
231 position, length and direction; ii) the global analysis performs a root system level analysis
232 and computes the total visible surface, convex hull, width and depth; iii) the shape analysis
233 uses Elliptic Fourier Descriptors or pseudo-landmarks similarly to RootScape¹³ to perform
234 a shape analysis on the root system iv) the directionality analysis computes the mean di-
235 rection of root particles in a root system (either on the full image or by user-defined region
236 of interest in the image). These four analysis methods are fully automated by default, but
237 can be manually adjusted if needed. The second module of GLO-RIA (RootReporter) was
238 specifically designed for the analysis of multi-layered images such as combinations of gene

239 reporter, root structure and soil moisture. Shortly, the plugin works as follow: i) detection
240 of the gene reporters and the structure reporters in their respective images; ii) if needed, a
241 manual correction can be performed to correct the automated detection; iii) gene reporters
242 are linked with the soil water content and the structure reporters, based on their proximity;
243 iv) gene reporter intensity (either absolute or normalized using the structural reporter) is
244 computed; v) all data are exported and saved to a RSML datafile¹⁴. Gene and structure
245 reporters can be followed across different time and space points. Using an object oriented
246 approach, great care has been taken to facilitate the user interactions on the different images
247 to streamline the analysis process. Table 2 shows a list of root system features extracted
248 using GLO-RIA. GLO-RIA does not currently have the ability to reconstruct the root archi-
249 tecture in itself (topological links between roots). This is a challenge for analyzing images
250 captured by GLO-Roots since soil particles cause disruption of root segments.

251 **Continuous imaging of root growth**

252 The size of our rhizotrons enables undisturbed root system development (before roots reach
253 the sides or the bottom of the rhizotron) for about 21-23 days for the Col-0 accession
254 growing under long day conditions (Figure 2); however root traits such as directionality
255 can be observed until later stages of plant development. See 35 DAS root system and
256 directionality in Figure 2A-B. An example of a time series spanning 11 to 21 days after
257 sowing (DAS) of Col-0 roots expressing *ProUBQ10:LUC2o* is shown in Fig 2A and [Video 1](#)
258 with a color-coded time projection shown in Fig 2C. Directionality analysis (Fig 2B) shows
259 a progressive change in root system angles from 0 ° (vertical) to 45 ° as lateral roots take
260 over as the predominant root type. Figure 2D shows the evolution over time of several root
261 traits that can be automatically captured by GLO-RIA (depth, width, area) and others
262 that can be manually quantified (primary root growth rate or number of lateral roots per
263 primary root).

264 Root system architecture of different *Arabidopsis* accessions.

265 The study of natural variation for root system architecture and root traits is a powerful
266 approach for understanding adaptive strategies plants use to cope with environmental change
267 and for identifying the genetic basis for such differences. In *Arabidopsis*, Quantitative Trait
268 Locus (QTL) and Genome-Wide Association Studies (GWAS) have led to the identification
269 of genes affecting root development¹⁵. However, traits are usually measured in seedlings
270 less than 2 week old. Selective pressures that affect allele frequencies in a population likely
271 act on genes that affect root system traits at later stages of the plant life cycle, as well.
272 As a proof of concept to estimate the utility of our root imaging system to phenotype
273 adult root system traits, we transformed a small set of accessions (Bay-0, Col-0 and Sha)
274 with the *ProUBQ10:LUC2o* reporter and quantified RSA at 22 DAS (Fig 3A-C). GLO-RIA
275 analysis of these root systems identified several root traits that distinguish Col-0, Bay-0
276 and Sha. Directionality analysis revealed an abundance of steep-angle regions in the root
277 system of Bay while Sha showed an abundance of shallow-angled regions and Col-0 was
278 intermediate (Fig 3D). Bay-0 shows the deepest and narrowest root system leading to the
279 highest depth/width ratio while Sha has the widest root system (Fig 3E). Other root traits
280 such as root system area and the vertical center of mass also showed significant differences
281 (Figure 3-figure supplement 1B). Broad sense heritability values for depth (96.3), area (92.0),
282 depth/width (97.8), width (95.7) and vertical center of mass (95.0) were all higher than
283 90%. To capture the richness of root architecture shape, we used GLO-RIA to extract
284 pseudo-landmarks describing the shape the root system to perform PCA analysis. The first
285 principal component separates Col-0 and Sha plants from Bay-0 ones capturing root systems
286 that vary in the distribution of widths along the vertical axis. (Fig 3F). While Bay-0 shows
287 an homogenous distribution of widths along the vertical axis, Sha and Col-0 are much wider
288 at the top than in the bottom. PC2 seems to be capturing a relationship between width at
289 the top and depth, slightly separating Sha root systems which are wide at the top and deep
290 from Col-0 root systems which are wide but not as deep as in Sha. Using shape information
291 extracted from EFDs we can distinguish the three different accesions using PCA analysis

²⁹² (Fig 3G)

²⁹³ **GLO-Roots for Brachypodium and Tomato**

²⁹⁴ To examine the general applicability of the GLO-Roots system for other species, we intro-
²⁹⁵ duced LUC2o-expressing reporters into the model grass *Brachypodium distachyon* and the
²⁹⁶ crop plant *Lycopersicon esculentum* (tomato). Brachypodium is well suited to the GLO-Root
²⁹⁷ system because, like Arabidopsis, its small size allows mature root systems to be studied in
²⁹⁸ relatively small soil volumes^{16,17}. *LUC2o* driven by the *ZmUb1* promoter was introduced into
²⁹⁹ Brachypodium using the pANIC vector¹⁸. Brachypodium roots showed a distinct architec-
³⁰⁰ ture from Arabidopsis marked by prolific development of secondary and tertiary lateral roots
³⁰¹ (Fig 4A). This is consistent with other studies that show that Brachypodium has a typical
³⁰² grass root system¹⁷. Comparison of root system development in rhizotrons with gel-based
³⁰³ media showed that root growth is higher in soil than in plates (Figure 4-figure supplement
³⁰⁴ 1). Previous work has suggested that auxin levels in Brachypodium roots is sub-optimal for
³⁰⁵ growth¹⁹. Pacheco-Villalobos and colleagues suggest that, in Brachypodium, and contrary
³⁰⁶ to what happens in Arabidopsis, ethylene represses *YUCCA* reducing the synthesis of auxin.
³⁰⁷ The reduced growth that we observe in plates and the high levels of ethylene that build up
³⁰⁸ in sealed plates²⁰ would support this mechanism.

³⁰⁹ Tomato plants were transformed with *Pro35S:PPyRE8o* and *ProeDR5rev:LUC2* reporters.
³¹⁰ The plants showed more rapid growth than Arabidopsis or Brachypodium and required fer-
³¹¹ tilizer to prevent obvious signs of stress (reduced growth, anthocyanin accumulation). Root
³¹² systems were imaged from 17 DAS plants. Roots showed less branching than Arabidopsis
³¹³ but many presumptive lateral root primordia marked by DR5-expression (Fig 4C-D). These
³¹⁴ results show that the GLO-Roots method can be applied to study root systems of plants
³¹⁵ and will likely be useful for studying root systems of other small to medium sized model
³¹⁶ plants and for early stages of larger crop plants.

317 **Spectrally distinct luciferases enable gene expression patterns, characterization**
318 **of root system interactions and microbial colonization.**

319 We tested whether spectrally distinct luciferase reporters would enable additional informa-
320 tion besides root architecture to be captured from root systems. Luciferase reporters have
321 been commonly used to study gene expression and these resources can potentially be utilized
322 to study these regulatory events in soil-grown roots. We transformed *ProACT2:PpyRE8o*
323 into two well studied LUC reporter lines: the auxin response reporter line *ProDR5:LUC*²¹
324 (Figure 5A-B) and the Reactive Oxygen Species (ROS) response reporter *ProZAT12:LUC*²²
325 (Figure 5C-D). We implemented in GLO-RIA an algorithm that semi-automatically identifies
326 gene reporter signal and associates this object to the corresponding root structure segment.
327 A graphical representation of the results obtained with Root Reporter can be observed in
328 Figure 5E. Reporter intensity values along the first 5 mm of root tips can also be observed in
329 Figure 5-figure supplement 1. We then took advantage of our ability to constitutively express
330 two spectrally different luciferases and imaged the overlapping root systems (one expressing
331 *ProUBQ10:LUC2o* and the other *ProACT2:PPy RE8o*). Root systems were distinguishable
332 using this system (Figure 5-figure supplement 2); measurements of root system area did not
333 reveal a significant effect on root growth when two plants were grown in the same rhizotron,
334 however further studies are warranted (Figure 5-figure supplement 2) The GLO-Roots sys-
335 tem uses non-sterile growth conditions, which allows complex biotic interactions that may
336 affect responses to the environment. Bacteria themselves can be engineered to express lumi-
337 nescent reporters through integration of the LUX operon, which results in luminescence in
338 the blue region of the spectrum and is thus compatible with the plant-expressed luciferase
339 isoforms we have tested. *Pseudomonas fluorescens* CH267²³, a natural Arabidopsis root
340 commensal, was transformed with the bacterial LUX operon and used to inoculate plants.
341 Thirteen days after inoculation we were able to observe bacterial luminescence colocalizing
342 with plant roots. *P. fluorescens* did not show an obvious pattern of colonization at the root
343 system scale level. As a proof-of-principle test of the multi-dimensional capabilities of the
344 GLO-Roots system we visualized both *LUC2o* and *PPyRE8o* reporters in plants and the

³⁴⁵ LUX reporter in bacteria in the same rhizotron (Figure 5-figure supplement 3).

³⁴⁶ **Adaptive changes in root system architecture under water deprivation, phos-**

³⁴⁷ **phorus deficiency and light** To test the utility of the GLO-Roots system to understand
³⁴⁸ response of root systems to environmental stimuli we tested the effects of light and condi-
³⁴⁹ tions that mimic drought and nutritional deficiency. To examine the effects of light exposure
³⁵⁰ on the root architecture, the black shields, which normally protect the soil and roots from
³⁵¹ light, were removed from the top half of the rhizotrons 10 DAS. Using directionality analysis
³⁵² we detected a significant increase in the steepness of roots only in the light exposed region of
³⁵³ the rhizotron, while the lower shielded region showed no difference. (Fig 7-figure supplement
³⁵⁴ 3A-B and Fig 7-figure supplement 4). Light can penetrate the top layers of soil²⁴ and it
³⁵⁵ has been proposed to have a role in directing root growth specially in dry soils²⁵ through
³⁵⁶ the blue light receptor *phot1*. Root directionality was not significantly different between
³⁵⁷ light and dark-treated roots of the *phot1/2* double mutant suggesting that blue light per-
³⁵⁸ ception is necessary for this response^{25,26} (Fig 7-figure supplement 3B-lower panel). These
³⁵⁹ data highlight the strong effects of light on root system architecture²⁷, which GLO-Roots
³⁶⁰ rhizotrons are able to mitigate.

³⁶¹ Plants grown in low-P soil showed a significant increase in the width-depth ratio of the root
³⁶² system compared to plants grown in P-replete soil, as determined using the automated root
³⁶³ system area finder in GLO-RIA (Fig 7-figure supplement 2A-B). Plants under P deficiency
³⁶⁴ showed an increase in the ratio between root-shoot area (Fig 7-figure supplement 2C) and
³⁶⁵ higher investment of resources in the development of the root system at the expense of shoot
³⁶⁶ growth (Fig 7-figure supplement 2D). Root systems of control and P-deficient plants showed
³⁶⁷ no significant differences in directionality at 22 DAS but at 27 DAS, roots were more hori-
³⁶⁸ zontally oriented in P-deficient plants (Fig 7-figure supplement 2E). The observed changes in
³⁶⁹ root architecture are consistent with root system ideotypes that improve phosphorus uptake
³⁷⁰ efficiency.

³⁷¹ GLO-Roots is especially well suited for studying water-deficit (WD) responses. First, shoots

372 are exposed to the atmosphere and vapor pressure deficit (VPD) is maintained at levels that
373 allow for transpiration of water from the shoot. Second, soil in rhizotrons is exposed to air
374 at the top and dries basipetally (from the top-down); drying soil increases the volume
375 occupied by air and reduces contact of root with liquid water, all of which are similar to
376 changes in soil expected in the field during WD. Finally, as peat-based soil dries, its optical
377 properties change, allowing moisture content to be approximated from bright-field images.
378 We took advantage of the change in gray-scale pixel intensity to construct a calibration
379 curve (Figure 6-figure supplement 1) that quantitatively relates gray-scale pixel intensity to
380 moisture content (Fig 6A); water content can be color coded in images with appropriate
381 look up tables (Fig 6B). Soil color was not affected by the presence or absence of roots
382 (Figure 6-figure supplement 2). Using this approach, water content in a rhizotron can be
383 mapped and visualized in 2D (Fig 6C-D). In the example shown, we can observe that a 22
384 DAS Bay-0 plant depleted soil-moisture content locally around the the root system (Figure
385 6E).

386 We performed several trials to simulate WD in our growth system. Plants were germinated,
387 grown under control conditions then transferred to 29°C and standing water removed from
388 the container holding the rhizotrons starting at 9 DAS or 13 DAS. Elevated temperature
389 combined with water deficit is a common stress that modern crops varieties are poorly
390 adapted to, thus highlighting the importance of examining this combined treatment^{28,29}.
391 Plants were maintained in this WD regime until 22 DAS when luciferin was added and the
392 plants were imaged. At 13 DAS, lateral roots near the soil surface are already emerged
393 ([Video 1](#), Figure 2A). After 9 days of water deficit treatment, lateral roots showed an in-
394 crease in gravitropism leading to the development of a root system that was deeper, more
395 vertically oriented and with more tertiary roots (Fig 7A). Roots of Bay-0 plants showed
396 similar responses though the extent of change was less pronounced since Bay-0 roots are
397 normally more vertically oriented (Fig 7B). Plants transferred at 9 DAS showed less lateral
398 root development in the top layer of soil (Fig 7E). At this time point, lateral roots start to
399 emerge ([Video 1](#)) and early drought may lead to growth quiescence or senescence. Careful
400 examination of roots in these regions showed evidence of small lateral root primordia pop-

401 ulating the primary root (Figure 7F). After 24 h of re-watering (Figure 7G) these lateral
402 root primordia reinitiated growth (Figure 7H).

403 Time-lapse imaging of the water deficit response showed that changes in root growth direc-
404 tion occurred ahead of the dry soil front [Video 3](#). Using GLO-RIA we were able correlate
405 water moisture contents with local orientation of the root segments. With this approach we
406 observed that root segments in dryer areas of rhizotron grew at steeper root angles (Figure
407 8) than roots in growing in well watered regions, though lateral root angle in wetter regions
408 was also affected. These data suggest that local and systemic signaling is likely involved in
409 redirecting lateral roots deeper during the simulated drought treatments tested here.

410 We also grew plants under WD at control temperatures or under WW conditions at elevated
411 temperature to test the effects of these individual stresses on root architecture. We observed
412 that both conditions were sufficient to induce a change in root directionality indicating that
413 the plant uses similar mechanisms to avoid heat and water-deficit associated stresses (Figure
414 7-figure supplement 1). We next asked which regulatory pathways controlled the observed
415 changes in lateral root directionality during simulated drought. Hydrotropism is a known
416 environmental response that directs root growth towards wet regions of soil. MIZ1 is an
417 essential regulator of hydrotropism; however *miz1* mutants had no significant effect on water
418 deficit-induced changes in root directionality, compared to wild type (Fig 7C), indicating
419 that this response was distinct from hydrotropism. Auxin is an important mediator of
420 gravitropism and auxin treatment causes lateral roots to grow more vertically⁷. Consistent
421 with this role for auxin, mutant plants with loss of function in the auxin receptor TIR1, did
422 not show changes in the root system directionality between WW and WD conditions (Fig
423 7D).

⁴²⁴ **Discussion**

⁴²⁵ **GLO-Roots enables a multi-dimensional understanding of root biology**

⁴²⁶ Recent studies of root systems has emphasized structural attributes as important contrib-
⁴²⁷ utors of root system function. Indeed, studies examining the role of genetic variants in
⁴²⁸ tolerating abiotic stress have demonstrated the importance of such characteristics. Roots,
⁴²⁹ however, are highly diverse in the biology they perform and a multi-dimensional understand-
⁴³⁰ ing of root systems, which incorporates differences in signaling, metabolism and microbial
⁴³¹ association as well as structure, may provide a clearer understanding of the degree to which
⁴³² sub-functionalization of the root system plays a role in important processes such as acclima-
⁴³³ tation and efficient resource acquisition.

⁴³⁴ We have developed tools in GLO-Roots that allow for tracking multiple aspects of soil
⁴³⁵ physicochemical properties and root biology simultaneously. Using GLO-Roots, we are able
⁴³⁶ to map in 2D coordinates soil physical properties such soil moisture together with root ar-
⁴³⁷ chitecture traits such as directionality, growth rates and gene expression levels. All this
⁴³⁸ information is aggregated in layers for each x, y coordinate. Using GLO-RIA we integrate
⁴³⁹ this multilayer information, leveraging our ability to simultaneously and seamlessly inves-
⁴⁴⁰ tigate root responses to environmental stimuli such as soil moisture content. Luciferase
⁴⁴¹ isoforms that emit light at different wavelengths allow for constitutive and regulated pro-
⁴⁴² moters to be studied together. Introduction of luciferase reporters into microbes provides
⁴⁴³ an additional layer of information that provides a readout on the association between or-
⁴⁴⁴ ganisms and how this might be affected by environmental conditions. The flexibility of the
⁴⁴⁵ GLO-Roots system may enable additional dimensionality to our understanding of root biol-
⁴⁴⁶ ogy. Other physical properties such as CO₂ or pH mapping in rhizotrons have already been
⁴⁴⁷ enabled by using planar optodes³⁰. It may be possible to engineer LUX-based reporters
⁴⁴⁸ in microbes that are responsive to extracellular metabolites, creating microbial biosensors,
⁴⁴⁹ and integration of such tools may enable root-exudation and nutrition to be analyzed in
⁴⁵⁰ soil. Split-Luciferase reporters have been engineered that allow bi-molecular interactions to
⁴⁵¹ be studied. Finally, molecular sensors analogous to FRET sensors, termed BRET-sensors³¹,

452 may allow metabolite tracking dynamically through the root system. With additional inno-
453 vation in the development of luciferase reporters, the GLO-Roots systems will likely expand
454 the repertoire of biological processes that can be studied over an expanded range of devel-
455 opmental time points and environmental conditions.

456 **Enhanced root growth and gravitropism may constitute an avoidance mechanism**
457 **used during drought**

458 It has been proposed that plants with steep root systems will be better able to tap into deep
459 water resources and thus perform better under water deprivation. For example in rice, the
460 IR64 paddy cultivar shows shallow root systems in upland fields whereas Kinandang Patong,
461 an upland cultivar, is deeper rooting⁸. Plants maintain a number of regulatory pathways that
462 mediate changes in physiology during WD. Enhanced growth of root systems has been well
463 characterized in field-grown plants; however this has not been recapitulated in studies of gel-
464 grown Arabidopsis plants. Thus, it has been unclear whether Arabidopsis simply responds
465 to WD differently. Our results here show that Arabidopsis does indeed maintain a classical
466 WD response that expands the root system and directs growth downward. Interestingly,
467 under our stress regime, we did not observe a significant decrease in the relative water
468 content of shoot tissues (Figure 7-figure supplement 5), suggesting that the changes in root
469 architecture were sufficient to provide access to deep water and prevent dehydration. Such
470 changes in root growth are likely regulated through systemic and local signaling that involve
471 auxin signaling but acts independently of known pathways that control moisture-directed
472 root growth.

473 **Perspectives and Conclusions**

474 Understanding plant biology requires a sophisticated understanding of how environmental
475 stimuli affect the form and function of plants as well as an understanding of how physiological
476 context informs such responses. Environmental conditions are at least as complex as the
477 plants they affect. Plant roots are exposed to a variety of environmental signals that change

478 in time and space at very different scales that are integrated at the whole plant system. It is
479 an important challenge in biology to develop methods of growing and studying plants that
480 present such stimuli in a manner that the plant is likely to encounter in nature. After all, the
481 plants we study have evolved to survive through mechanisms that have been selected, over
482 evolutionary time, in nature. It will be interesting for future studies to determine how other
483 environmental stimuli affect root growth using GLO-Roots and whether these responses
484 differ between accessions of Arabidopsis. Identification of the genetic loci responsible for
485 phenotypic variation in adult root phenotypes may identify the molecular basis for adaptive
486 variation that exists in this species and potentially identify loci that are useful for breeding
487 efforts needed for the next green revolution.

488 Materials and methods

489 Growth system

490 **Rhizotrons and growth system fabrication.** Rhizotrons are composed of two sheets of
491 1/8" abrasion resistant polycarbonate plastic (Makrolon AR (R)) cut to size using a water
492 jet (AquaJet LLC, Salem, OR), two acrylic spacers cut using a laser (Stanford Product
493 Realization Lab), two rubber U-channels cut to strips 30 cm long ([McMaster Carr part](#)
494 [# 8507K33](#)) and two sheets of black 0.030" thick polypropylene sheets ([McMaster Carr](#)
495 [part # 1451T21](#)) cut with a straight-edge razor blade. Rhizotron designs were drafted in
496 Adobe Illustrator (Adobe, San José, CA). The blueprints of all the parts are provided in
497 Supplement 1. The top edge of each polycarbonate sheet was painted with black 270 Stiletto
498 nail polish (Revlon, New York, NY).

499 **Boxes and holders.** Rhizotrons are held vertical during plant growth in a custom rack sys-
500 tem composed of two sheets of 1/4" black acrylic plastic cut with slots for eleven rhizotrons
501 using a laser, four 3/8" PVC rods ([McMaster Carr part # 98871a041](#)) secured with PVC
502 nuts ([McMaster Carr part # 94806a031](#)) to hold the acrylic sheets horizontal. The rack is
503 placed inside a 12" x 12" x 12" black polyethylene tank ([Plastic Mart part # R121212A](#)).

504 **Rhizotron preparation** The procedure to construct a rhizotron with soil is as follows:
505 Two pieces of polycarbonate plastic are laid flat on a table with the spacers inserted. Using
506 an electric paint gun, a fine mist of water is applied to the bare polycarbonate sheets. Then,
507 using a 2 mm sieve (US Standard Sieve Series N° 10) a fine layer of PRO-MIX(r) PGX soil
508 (Premier Tech, Canada) is applied. Excess soil is discarded by gently tapping the plastic
509 against the table in a vertical position. Water is sprayed again onto the soil, then a second
510 layer of Pro-MIX is applied as before. For P deficiency experiments soil supplemented with
511 1 ml of 100 µM P-Alumina (control) and 0-P-Alumina (P deficient) was used. To prevent
512 the soil from falling out of the bottom opening, a 3 x 6 cm piece of nylon mesh is rolled into
513 a 1 cm wide tube and placed at the bottom side of the rhizotron. The spacers are removed
514 and replaced by clean spacers. The two faces of the rhizotron are carefully joined together
515 and two rubber U-channels slipped on to clamp all pieces together. Assembled rhizotrons
516 are placed into the rack inside the boxes and 500 mL of water is added to the box.

517 **Plant growth** *Arabidopsis thaliana* seeds were stratified for 2 d at 4 °C in Eppendorf tubes
518 with distilled water. Seeds were suspended in 0.1 % agar and 5 to 10 were sown using
519 a transfer pipette in the rhizotron. A transparent acrylic sheet was mounted on top of
520 the box and sealed with tape to ensure high humidity conditions that enable *Arabidopsis*
521 germination. Three days after sowing, the cover was unsealed to decrease humidity and
522 allow the seedlings to acclimate to a dryer environment. From 3 days after sowing (DAS)
523 to the time the first true leaves emerged, it was critical to ensure that the top part of the
524 rhizotron remained humid for proper germination of the plants. Between three and five DAS
525 the rhizotrons were thinned leaving only the number plants required for that experiment,
526 typically one, except for experiments examining root-root interactions. Unless otherwise
527 stated, all the experiments presented here, treatments were started 10 DAS. Plants were
528 grown under long day conditions (16 h light / 8 h dark) using 20–22 °C (day/night) and
529 150 µE m⁻¹ s⁻¹. Two types of growth environments were used for experiments. A walk-in
530 growth chamber with fluorescent lightning and a growth cabinet with white LED lights.
531 Relative water content measurements were done as previously described³²

532 **qRT-PCR analysis.**

533 Seeds were surface sterilized as described before² and grown in rhizotrons, 100 cm³ pots, or
534 on two types of 1% agar (Duchefa) media containing either 1x MS nutrients (Caisson) and 1%
535 Sucrose, (termed ms media) or ¼x MS nutrients only (termed ms25 media). Both media were
536 buffered using 0.5 g/L MES and pH was adjusted to 5.7 with KOH. All plants were grown
537 together in a growth cabinet with LED lights under long day conditions (16h day/8h night).
538 Root and shoot tissue was collected separately from individual plants at the end of the day
539 (1 hour before the lights shut off) and at the end of the night (1 hour before lights came on).
540 Three biological replicates were collected for each condition. RNA was extracted using the
541 Plant RNA MiniPrepTM kit (ZYMO Research) according to manufacturer's instructions
542 with on-column DNase treatment (Qiagen). cDNA was made using the iScript Advanced
543 cDNA Synthesis for RT-qPCR kit (Bio-Rad) from 200 ng of total RNA. qRT-PCR was
544 performed using a Fluidigm BioMarkTM 96.96 Dynamic Array IFC with the EvaGreen®
545 (Bio-Rad) fluorescence probe according to the Fluidigm Advanced Development Protocol
546 number 37. For the analysis, all the reactions with no amplification (Ct =999) were either
547 removed (if the other technical duplicate amplified) or set to the maximal Ct for that assay
548 type. The two technical replicates were then averaged and dCt values calculated using
549 AT3G07480, AT4G37830, At1g13320 and At1g13440 as reference internal controls. PCA
550 plots were generated with Devium Web³³ using log dCt values. Primers used are listed in
551 file Supplement 8.

552 **Biological components**

553 **Codon optimization of luciferases.** The following luciferases that emit light at different
554 wavelengths were codon optimized for *Arabidopsis* (Genscript, Piscataway, NJ): LUC2: a
555 yellow improved version (Promega, Madison, WI) of the original *Photinus pyralis* (firefly)
556 LUC.

- 557 • Ppy RE8: a red variant³⁴ of the *P. pyralis* thermostable variant Ppy RE-TS³⁵.

- 558 • CBG99: a green variant (Promega, Madison, WI) from yellow click beetle (*Pyrophorus*
559 *plagiophthalmus*) luciferases.
- 560 • CBR: a red variant (Promega, Madison, WI) from yellow click beetle.

561 **Non-optimized luciferases.** We also used the following non-optimized luciferases:

- 562 • nanoLUC: a blue luciferase isolated from a deep sea shrimp³⁶.
- 563 • venusLUC2: a venus-LUC2 fusion reported to show higher luminescence output than
564 LUC2¹¹.
- 565 • A transposon containing the bacterial luciferase-containing LUX operon was inte-
566 grated into the *Pseudomonas fluorescens* CH267²³ genome by conjugation with *E.*
567 *coli* SM10 *pir* containing pUT-EM7-LUX³⁷ and used to track root microbe coloniza-
568 tion. For inoculation 9 DAS plants were inoculated with 2 mL of an overnight bacterial
569 culture resuspended in 10 mM MgSO~4 and diluted to 0.01 OD.

570 **Generation of single-reporter transgenic plants.** We generated transcriptional fu-
571 sions of all luciferases to constitutive promoters to examine the activity level and emission
572 spectrum of each isoform. The *attL1-attL2** entry clones containing plant-codon optimized
573 coding sequence of *LUC2*, *PpyRe8*, *CBG99* and *CBR* were synthesized by Genscript. A
574 DNA fragment including the *UBQ10* promoter region and first intron was amplified from
575 Col-0 genomic DNA with primers incorporating the attB1, attB4 combination sites at the 5'
576 and 3' respectively. The PCR product was then introduced into pDONR™ P4-P1R (Invitro-
577 gen) through a classic Gateway BP-reaction. The resulting plasmid, the *attL1-attL2* entry
578 clones with luciferase sequences, an empty *attR2-attL3** entry clone and the destination
579 vector dpGreenmCherry² were used to construct *ProUBQ10:LUC2o*, *ProUBQ10:PpyRE8o*,
580 *ProUBQ10:CBG99o* and *ProUBQ10:CBRo* through Gateway LR reactions. The destination
581 vector *dpGreenmCherry* contains a plasma membrane-localized mCherry coding sequence
582 driven by the 35S promoter and is used as a selectable marker of transformation at the

583 mature seed stage². We used Golden Gate cloning and the destination vectors that we had
584 generated before¹² for the following fusions: *ProUBQ10:nanoLUC2*, *ProUBQ10:venusLUC*,
585 *ProACT2:PpyRE8o*. Briefly, the different components of each construct were PCR ampli-
586 fied with complementary BsaI or SapI cutting sites, mixed with the destination vector in
587 a single tube, digested with either BsaI or SapI, ligated with T4 DNA ligase, then trans-
588 formed into *E. coli* Top10 cells and plated on LB antibiotic plates containing X-gal as pre-
589 viously described¹². Junction sites were confirmed by sequencing. We used pSE7 (Addgene
590 ID #: pGoldenGate-SE7: 47676) as the destination vector of the *ProUBQ10:nanoLUC2*,
591 *ProUBQ10:venusLUC* constructs and pMYC2 (Addgene ID #: pGoldenGate-MCY2: 47679)
592 as the destination vector for *ProACT2:PpyRE8o*. Maps of all the vectors can be found in
593 Supplement 8. *ProUBQ10:LUC2o* was transformed into Col-0, Bay and Sha accessions, the
594 *tir1-1*³⁸ mutant and the *miz1*³⁹ T-DNA insertion line (SALK_126928).

595 **Brachypodium distachyon** The *Arabidopsis* plant-codon optimized Luciferase gene,
596 *LUC2o*, was inserted into the monocot vector pANIC10 via Gateway cloning¹⁸. *Brachy-*
597 *podium distachyon* plants were transformed using the method of Vogel and Hill⁴⁰.

598 **Tomato** The transcriptional fusion *ProeDR5:LUC2* was generated by cloning the
599 *ProeDR5:LUC2* DNA fragment into the pBIB expression vector via restriction sites SalI
600 and Acc65I. The eDR5 promoter is an enhanced version of DR5 containing 13 repeats of
601 the 11-nucleotide core DR5 element⁴¹ and the pBIB expression vector contains an NPTII
602 resistance gene under the control of the NOS promoter for use as a selectable marker during
603 transformation. All tomato transformations were performed by the Ralph M. Parsons
604 Foundation Plant Transformation Facility (University of California, Davis).

605 **Generation of dual-reporter plants.**

606 To generate dual-reporter plants expressing luciferase isoforms that emit light with di-
607 vergent emission spectra we used *ProACT2:PpyRE8o* as the root structural marker and
608 ZAT12:LUC²² and DR5:LUC+²¹ lines that were transformed with the *ProACT2:PpyRE8o*

609 construct. All constructs were transformed using a modified floral dip method as described
610 in².

611 *Tomato*

612 The *Pro35S:PpyRE8o* transcriptional fusion was generated by putting the plant-codon op-
613 timized coding sequence described above into the pMDC32 expression vector through a
614 Gateway LR reaction. The pMDC32 vector contains a hygromycin resistance gene under
615 the control of the 35S promoter for use as a selectable marker during transformation. This
616 construct was transformed into the transgenic *ProeDR5:LUC2* tomato line.

617 **In vivo emission spectra of plants constitutively expressing luciferase isoforms.**

618 To generate *in vivo* emission spectra of all constitutively expressed luciferases, seeds were
619 sterilized and sown on MS plates as described before². After 8 days, seedlings were treated
620 with a 100 µM luciferin solution, incubated at room temperature for 3 hours and imaged
621 using an IVIS Spectrum imaging system (Perkin Elmer, bla, bla) using 20 nm band-pass
622 emission filters at the following wavelengths (in nm: 490-510, 510-530, 530-550, 550-570,
623 570-590, 590-610, 610-630, 630-650, 650-670, 670-690, 690-710). Raw images were analyzed
624 using Fiji and *in vivo* emission spectra were constructed. The full emission spectra of LUX
625 and nanoLUC could not be constructed since the maximum of these two luciferases is below
626 the lower band pass filter that were available.

627 **Imaging system**

628 We designed a custom imaging system (GLO1, Growth and Luminescence Observatory 1)
629 optimized for imaging dual-reporter luciferase expression in our custom rhizotrons. The
630 design was a joint effort with Bioimaging Solutions (San Diego, CA) who also built the
631 system and wrote the acquisition software that drives all the mechanical parts of the system.
632 The system is composed by two 2048 x 2048 PIXIS-XB cameras (Princeton Instruments,
633 Trenton, NJ) mounted on top of each other to capture two fields of view encompassing
634 approximately two 15 x 15 cm areas corresponding to the top or bottom of the rhizotron.

635 The cameras are fitted with a Carl-Zeiss macro lens. A filter wheel with space for four,
636 76.2 mm filters is positioned in front of the cameras and controlled by a stepper motor
637 allowing for automated changing of the filter wheel position. We used two -542/50 and
638 450/70- custom cut Brightline(R) band-pass filters (Semrock, Rochester, NY). In single
639 color imaging mode, the filter wheel is operated without filters. Positioned in front of the
640 filter wheel is a removable rhizotron holder mounted on a stepper motor. This stepper motor
641 is also controlled by the GLO-1 software allowing automatic acquisition of images from both
642 sides of the rhizotron sequentially. The whole imaging system is enclosed in a light-tight
643 black box with a door that allows loading and un-loading of rhizotrons.

644 **Plant Imaging**

645 Around 50 mL of 300 μ M D-luciferin (Biosynth, Itasca, IL) was added to soil at the top of
646 the rhizotron. In general 5 min exposures were taken per rhizotron, per side, per channel.
647 For daily imaging experiments, plants were imaged at dawn (+/- 1 hr) to reduce possible
648 effects on diurnal rhythms of keeping plants in the dark during imaging. Shoot images were
649 taken using a Nikon D3100 camera.

650 **Image Preparation**

651 Four individual images are collected: top front, bottom front, top back and bottom back.
652 Using an automated [ImageJ macro](#), a composite image is generated as follows: 1) To correct
653 for differences in background values between the two cameras the mean background value
654 of each image is subtracted from 200; 2) images are rotated and translated to control for
655 small misalignments between the two cameras; 3) the top and bottom images of each side
656 are merged; 4) the back image is flipped horizontally; 5) the front and back images are
657 combined using the maximum values. When dual color images are acquired this operation
658 is repeated for each channel. The final images produced are 16-bit depth and 4096 x 2048
659 pixels. The scale of the images is 138.6 pixels per cm. Considering that an Arabidopsis
660 roots is 100 μ m this results in 1.39 pixels across an Arabidopsis root.

661 **GLO-RIA imageJ plug-in**

662 GLO-RIA uses a combination of existing tools to extract relevant root architecture features.
663 Directionality is acquired using the [directionality plugin](#) from ImageJ. After the number of
664 direction bins (we usually use bins of 2 °) is defined by the user, a 5x5 sobel operator is used
665 to derive the local gradient orientation. This orientation is then used to build a distribution
666 of directions by assigning the square of the orientation into the appropriate bin. Instead of
667 representing the total counts at each orientation a relative value is calculated by dividing
668 the individual values at each bin by the total sum of the histogram (and multiplying by 100).
669 Similar algorithms have been used to quantify dynamic changes in the plant cytoskeleton⁴².
670 The Elliptic Fourier Descriptors are aquired using the [Fourier Shape Analysis plugin](#) on
671 convex hull shape of the root system. Elliptic Fourier Descriptors have been used in numer-
672 ous studies to analyse variations in shapes, notably in leaves (e.g⁴³) The shape analysis is
673 inspired by RootScape¹³. Due to the absence of fixed, recognisable structures in root system
674 (that are required for the position of true landmarks), pseudo-landmarks are automatically
675 extracted from the root systems. Shortly, the image is divided vertically at equidistant posi-
676 tions (with the number defined by the user) and for each of the image stripes, the minimum
677 and maximum x coordinates are computed. The shape analysis is therefore able to discrim-
678 inate root system with different vertical root distributions or global root system orientation
679 (e.g. chemotropism) . The code source for the plugin, manual and sample images can be
680 found in the [github repository](#) of the project.

681 Statistical analysis was performed in R⁴⁵. The tidyR⁴⁶, dplyr⁴⁶, gridExtra⁴⁷, shapes⁴⁸,
682 geomorph⁴⁹ and ggplot2⁵⁰ packages were used for data preparation, analysis and plotting.
683 Final figure preparation was done in [Inkscape](#).

684 **Data availability**

685 All the scripts and original data used to analyze and produce the images can be accessed
686 in the Github repository of the project: github.com/rr-lab/glo_roots. Raw files of all the
687 images used in the paper are availabe in [Dryad](#).

688 **Acknowledgements**

689 Work in the lab of JRD was funded by the Carnegie Institution for Science Endowment
690 and grants from the National Science Foundation (MCB-115795) and Department of En-
691 ergy, Biological and Environmental Research program (DE-SC0008769). RRA was sup-
692 ported by a Carnegie Postdoc Fellowship and currently by Conacyt Ciencia Básica Joven
693 Investigador grant number (CB-2014-01-238101). GL was supported by the Belgian Fonds
694 de la Recherche Scientifique. JM was funded by the National Science Foundation (IOS-
695 0820854). CH is funded by MGH Toteston & Fund for Medical Discovery Fellowship grant
696 2014A051303 and NIH R37 grant GM48707 and NSF grant MCB-0519898 awarded to Fred-
697 erick Ausubel, and previously by the Gordon and Betty Moore Foundation through Grant
698 GBMF 2550.01 from the Life Sciences Research Foundation. JV was funded by the Office
699 of Biological and Environmental Research, Office of Science, US Department of Energy, in-
700 teragency agreements DE-SC0001526 and DE-AI02-07ER64452. We thank Robert Mittler
701 and Philip Benfey for providing seeds of ZAT12:LUC and DR5:LUC+ respectively. We also
702 thank Neil Robbins for critical review of the manuscript and suggestions during the devel-
703 opment of the project. We greatly appreciate Tim Doyle's advice and help with luciferase
704 imaging.

705 **Competing interests**

706 We do not have any competing interests that we are aware of.

707 **Tables**

708 **Table 1:** Luciferases used in this study.

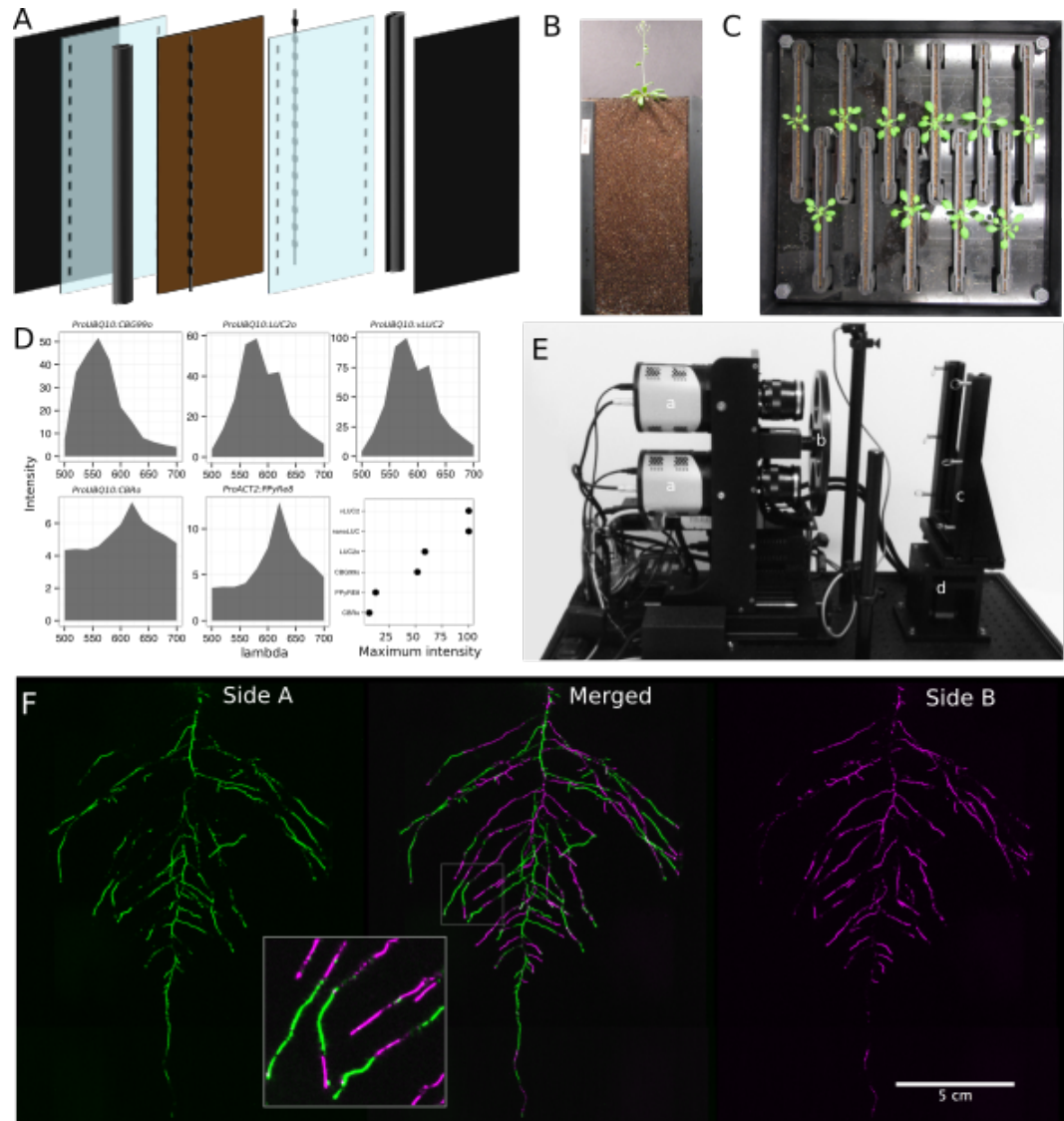
Luciferase	Origin	maximum wavelength	Substrate
Ppy RE8	firefly	618	D-luciferin
CBGRed	click beetle	615	D-luciferin

Luciferase	Origin	maximum wavelength	Substrate
venus-LUC2	FP + firefly	580	D-luciferin
LUC(+)	firefly	578	D-luciferin
CBG99	click beetle	537	D-luciferin
lux operon	A. fischeri	490	biosynthesis pathway encoded within operon
nanoLUC	Deep sea shrimp	470	furimazine

709 **Table 2:** list of root system features extracted using GLO-RIA.

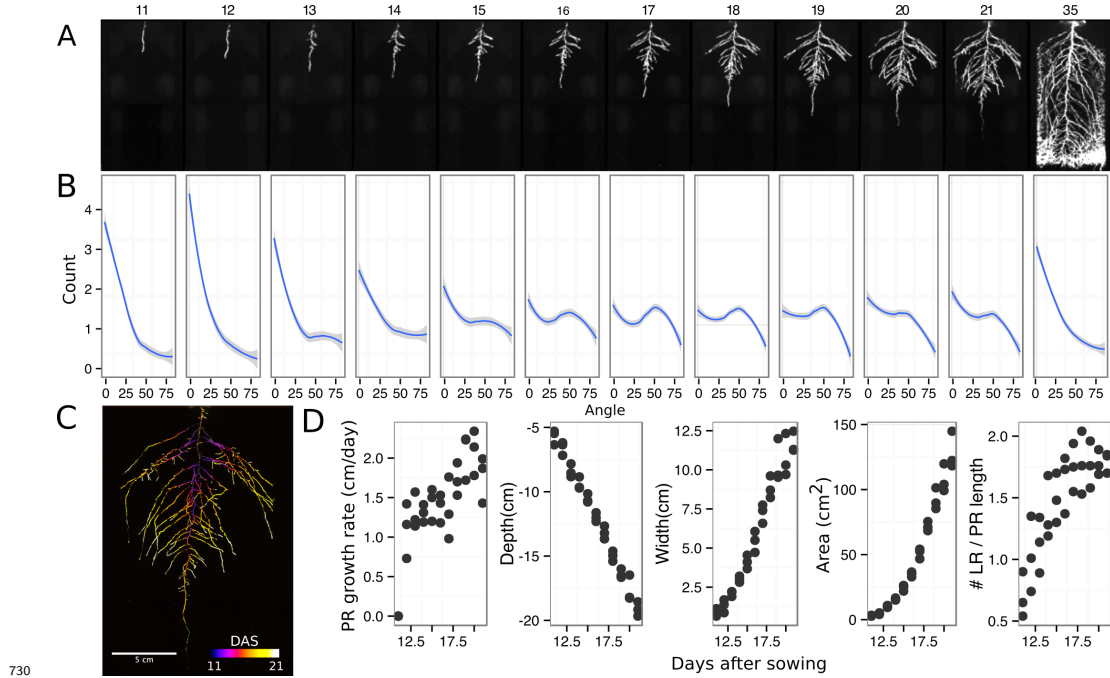
variable	unit
projected area	cm ²
number of visible roots	-
depth	cm
width	cm
convex hull area	cm ²
width	cm
feret	cm
feret angle	°
circularity	-
roundness	-
solidity	-
center of mass	cm
Directionality	°
Euclidean Fourier Descriptors	-
Pseudo landmarks	-

710 **Figures**



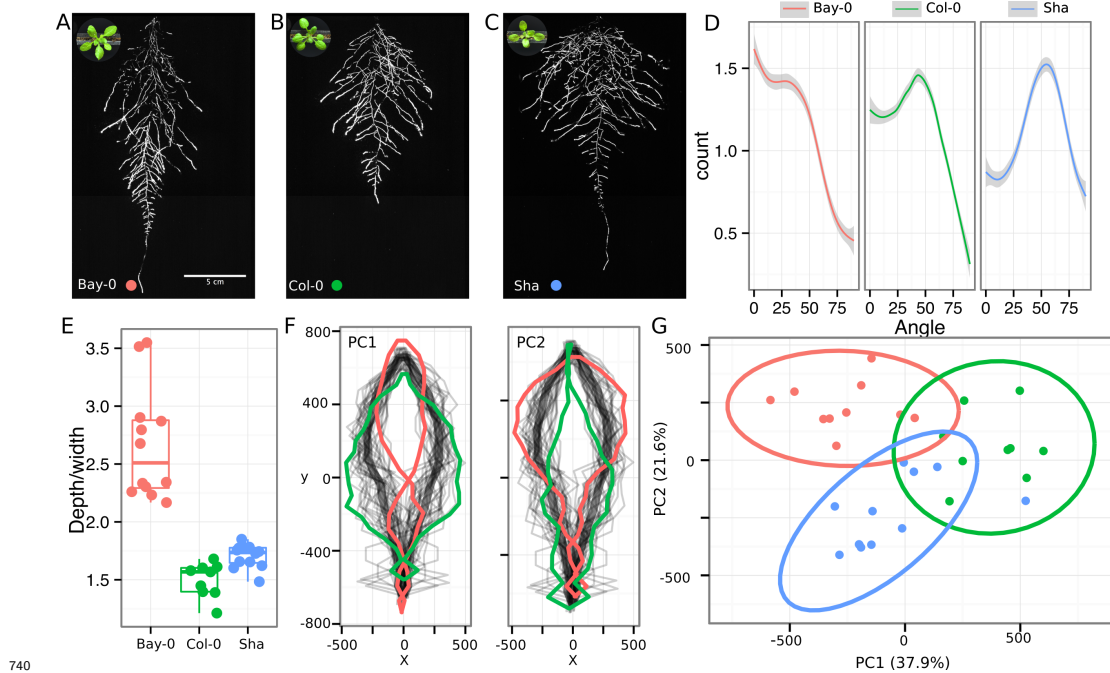
711
 712 **Figure 1.** A) 3D representation of the different components of the rhizotron: plastic
 713 covers, polycarbonate sheets, spacers and rubber U-channels. Blueprints are provided in
 714 Supplementary material 1. In brown, soil layer. B) Thirty five days old plant in rhizotron
 715 with black covers removed. C) Top view of holding box with eleven rhizotrons. D) In vivo
 716 emission spectra of different luciferases used in this study. Transgenic homozygous lines
 717 expressing the indicated transgenes were grown on agar media for 8 days. Luciferin (300

718 μM) was sprayed on the seedlings and plates were kept in the dark and then imaged for 2 s
 719 at wavelengths ranging from 500 to 700 nm. Five intensity values were taken from different
 720 parts of the roots of different seedlings and averaged. Relative maximum intensity values
 721 are indicated in the lower right graph. E) GLO 1 imaging system. The system is composed
 722 by two back illuminated CCD cameras (a) cooled down to -55°C . A filter wheel (b) allows
 723 for spectral separation of the different luciferases. On the right, a rhizotron holder (c) is
 724 used to position the rhizotrons in front of the cameras. A stepper motor (d) rotates the
 725 rhizotron 180° to image both sides. F) A 21 DAS plant expressing *ProUBQ10:LUC2o* was
 726 imaged on each of two sides of the rhizotron; luminescence signal is colorized in green or
 727 magenta to indicate side. In the middle of the panel, a combined image of the two sides
 728 is shown. The inset shows a magnified part of the root system. FW: fresh weight, PR:
 729 Primary root.



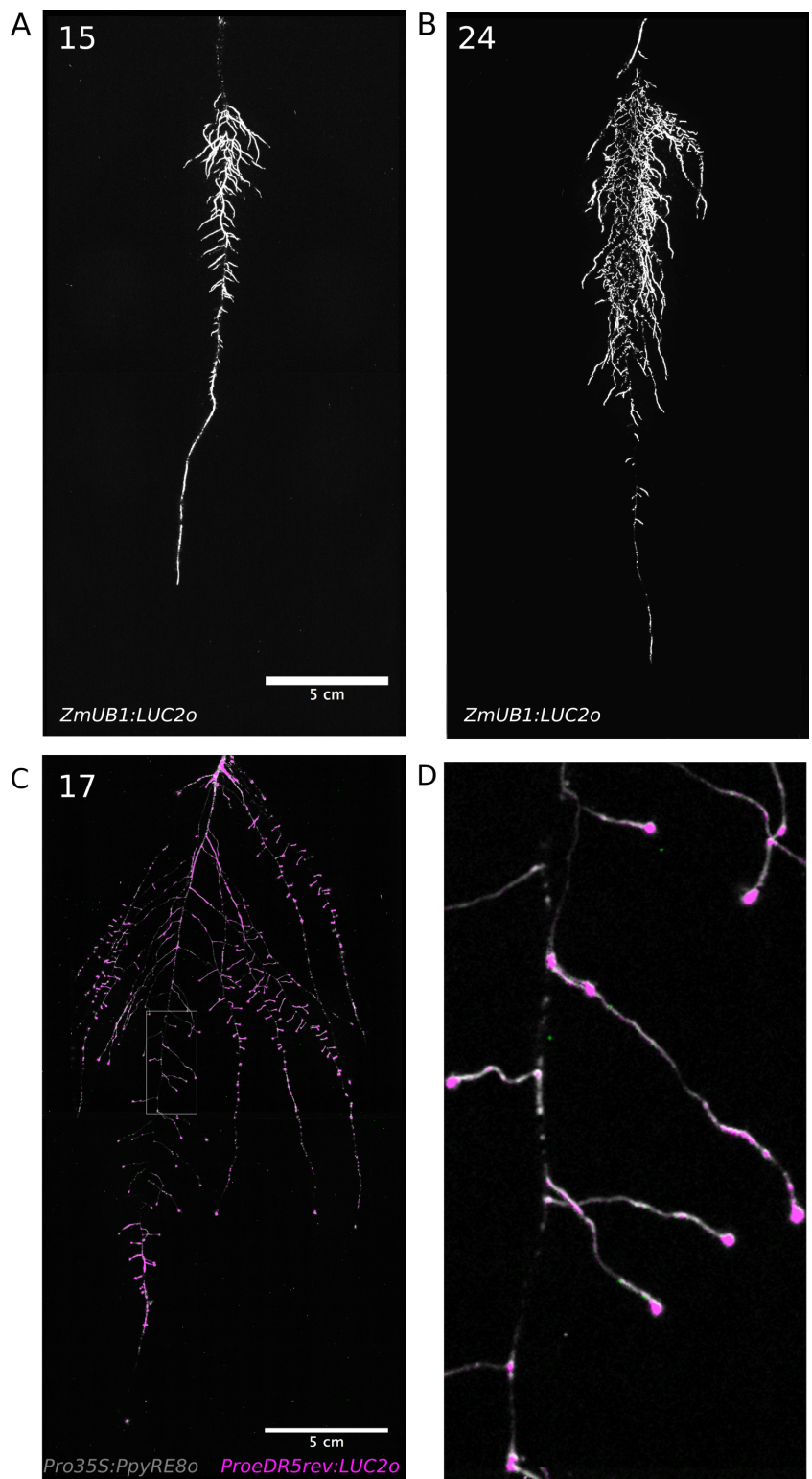
730 **Figure 2:** A) Typical daily time-lapse image series from 11 to 21 DAS of a
 731 *ProUBQ10:LUC2o* Col-0 plant. B) Directionality of the root system of plants in
 732 panel A calculated using the directionality plugin implemented in GLO-RIA. C) Color
 733 coded projection of root growth using the images in panel A. D) Primary root growth
 734 parameters.

735 rate, depth, width, root system area are automatically calculated from the convex hull,
 736 which is semi-automatically determined with GLO-RIA. Lateral root number and number
 737 of lateral roots divided by the primary root length were quantified manually. A Local
 738 Polynomial Regression Fitting with 95% confidence interval (grey) was used to represent
 739 the directionality distribution curve. (0° is the direction of the gravity vector).



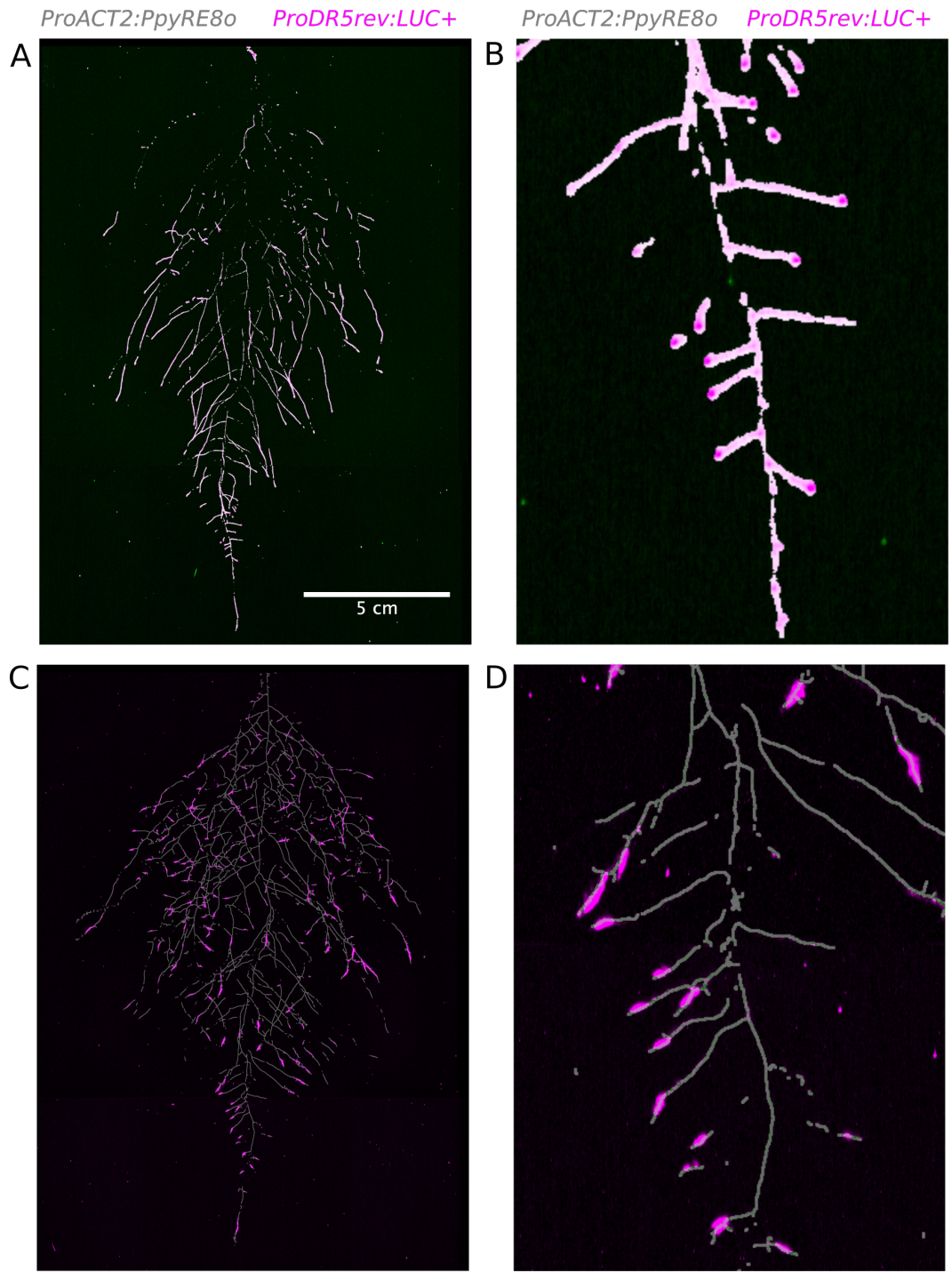
740
 741 **Figure 3.** Representative root and shoot images of A) Bay-0, B) Col-0 and C) Sha acce-
 742 sions 22 DAS transformed with *ProUBQ10:LUC2o*. D) Directionality of the root systems, E)
 743 depth/width ratio, F) Elliptic Fourier Descriptors of shape variation in root system architec-
 744 ture. Eigenvalues derived from the analysis of 9-12 plants per accession is shown. The first
 745 two Principal Components explaining 38% (PC1) and 22% (PC2) of the shape variation are
 746 plotted. PC1 captures homogeneity of root system width along the vertical axis with and
 747 PC2 a combination of depth and width in top parts of the root sytem. Red and green lines
 748 indicate -3SD and +3SD, respectively G) PCA separation of the different ecotypes using
 749 the PC described in F. A Local Polynomial Regression Fitting with 95% confidence interval
 750 (grey) was used to represent the directionality distribution curve. (0° is the direction of the
 751 gravity vector). Wilcoxon test analysis with $p < 0.01$ was used to test significant differences

⁷⁵² between the different accession (n = 9-12 plants).



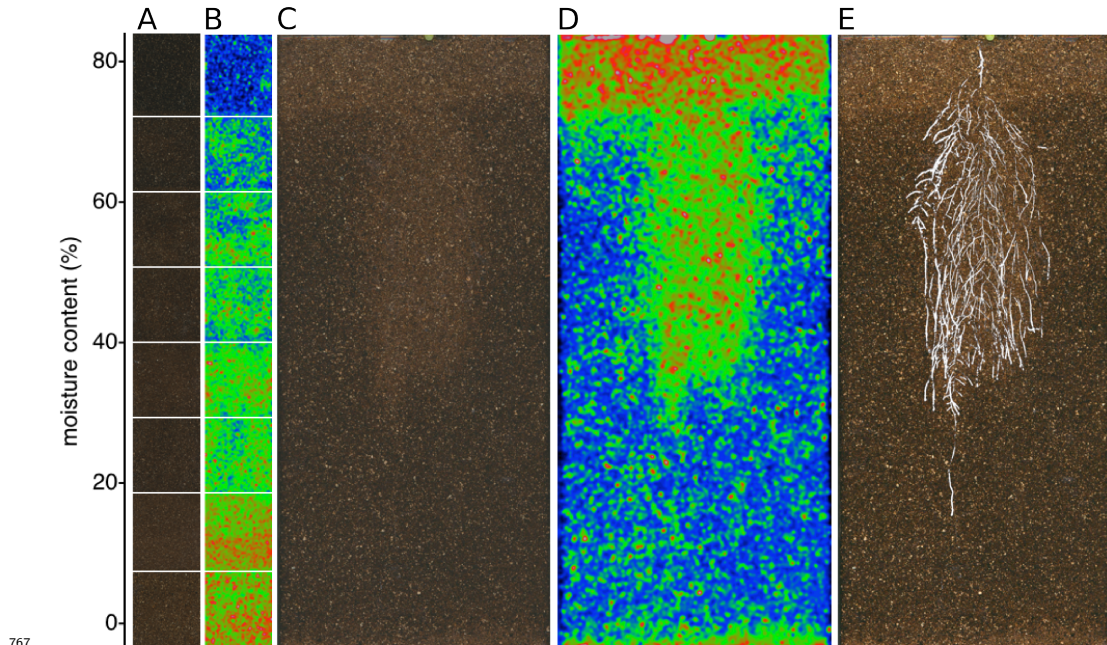
753

754 **Figure 4:** Roots of *Brachypodium distachyon* transformed with *ProZmUB1:LUC2o* and
755 imaged at 15 (A) and 24 (B) DAS grown in control conditions. C) 17 DAS tomato plant
756 transformed with *ProeDR5rev:LUC2o* (magenta) and *Pro35S:PPyRE8o* (grey) D) Zoomed
757 inset of root in panel D showing increased expression of *ProeDR5rev:LUC2o* reporter in
758 early-stage lateral roots.

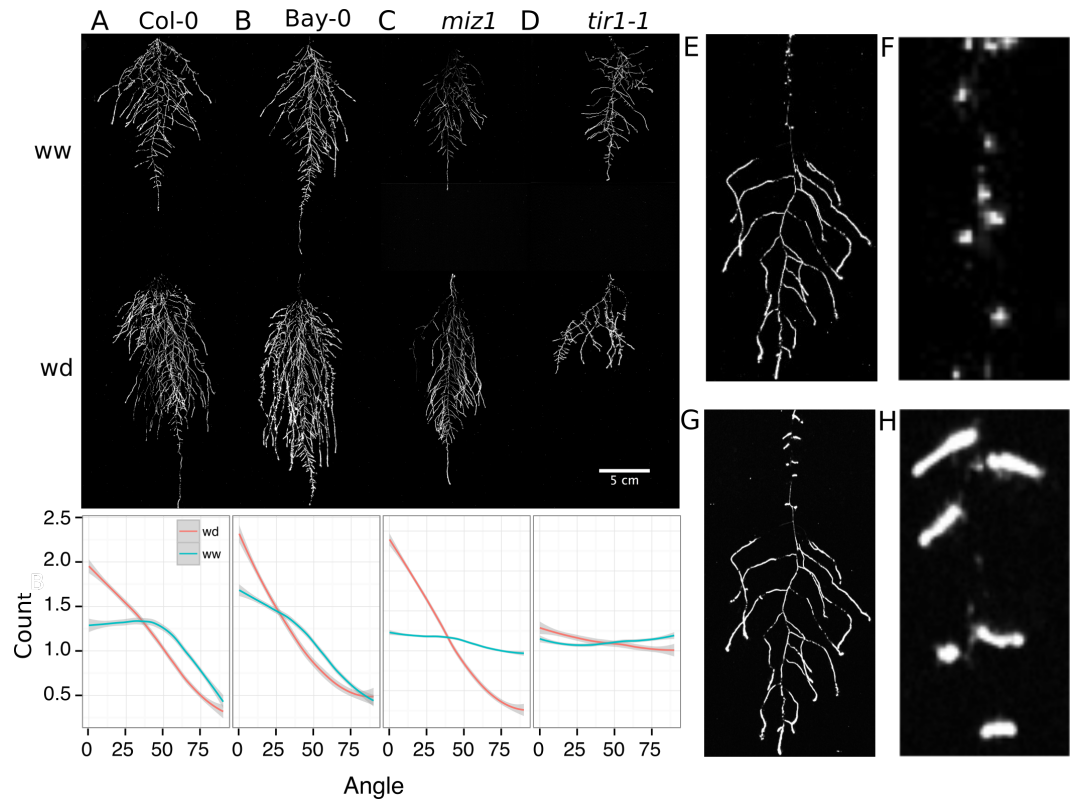


760 **Figure 5:** Images of whole root systems (A, C) or magnified portion of roots (B, D) at 22
761 DAS expressing *ProDR5rev:LUC+* (magenta, A, B) or *ProZAT12:LUC* signal (magenta,

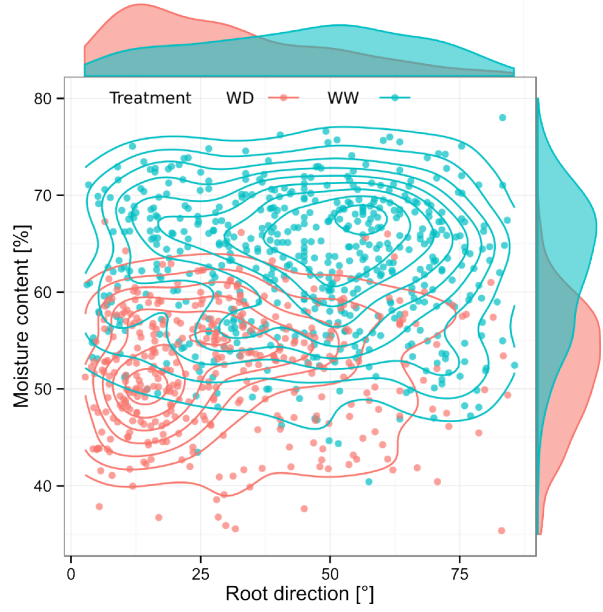
762 C, D)with skeletonized representation of roots generated using the *ProACT2:PpyRE80*
763 reporter expression (in grey). E) Visualization of the results obtained by analyzing the
764 ZAT12:LUC image with the GLO-RIA Root Reporter module. Blue circles are proportional
765 in size to the ZAT12:LUC intensity value. Hovering over the points will reveal numerical
766 values for the ZAT12:LUC intensity



767
768 **Figure 6:** Soil moisture mapping in rhizotrons. A) Composite image strip made from
769 rhizotrons prepared with different soil moisture levels. B) Differences in grey-scale intensity
770 values were enhanced using a 16-color Look Up Table (LUT). Brightfield image of soil in
771 rhizotron (C) and converted using 16-color LUT to enhance visualization of distribution of
772 moisture (D) . E) Root system of a Bay-0 22 DAS and subjected to water deprivation since
773 13 DAS. Root system visualized using luminescence and overlaid on brightfield image of soil
774 in (C).



775 **Figure 7:** A-D) Root systems 22 DAS and exposed to water deficit 13 DAS onwards.
 776 Sample images of well watered (left panels) and water deficit (right panels) root systems
 777 started 13 DAS and directionality (line graphs to left of images) for (A) Col-0 (B) Bay-0
 778 (C) *miz1* mutant and (D) *tir1-1*. E) Root system of a 22 DAS plant exposed to water
 779 deprivation from 9 DAS onwards with magnified view of lateral root primordia (F). G) The
 780 same root as in (E) 24 hours after rewatering and magnified view of lateral root primordia
 781 (H). Kolmogorov-Smirnov test at $p < 0.001$ was used to compare directionality distributions
 782 between the different treatments and genotypes. A Local Polynomial Regression Fitting
 783 with 95% confidence interval (grey) was used to represent the directionality distribution
 784 curve. (0° is the direction of the gravity vector).



786 **Figure 8:** Relationship between local soil moisture content and root growth direction. Data
 787 quantified from the time lapse shown in [Video 3](#). Density plots shown at periphery of graph
 788 for root direction (x-axis) and soil moisture (y-axis). (0° is the direction of the gravity
 789 vector).
 790

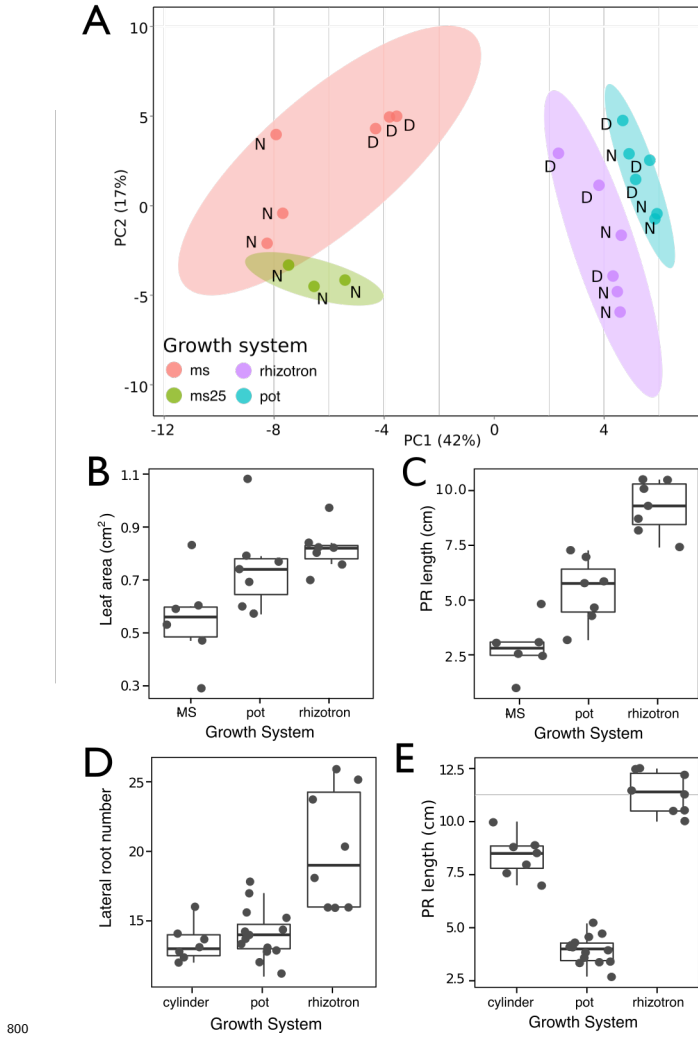
791 Videos

792 [Video 1](#) Time lapse from 11 to 21 DAS of a Col-0 plant expressing *ProUBQ10:LUC2o*
 793 grown in control conditions

794 [Video 2](#) 24 h time lapse a Col-0 plant expressing *ProACT2:PpyRE8* (gray) and *ZAT12:LUC*
 795 (magenta) after addition of a 1 M solution of NaCl on the right side of the plant.

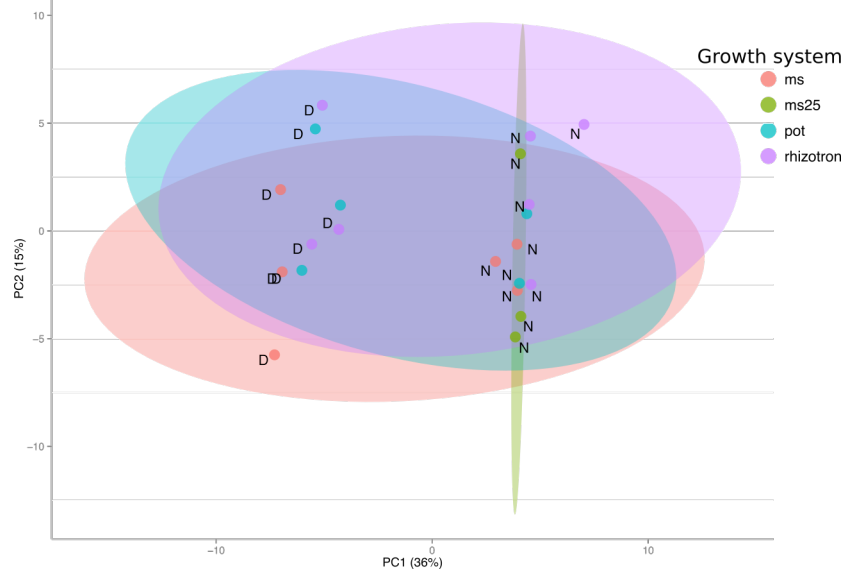
796 [Video 3](#) Time lapse from 16 to 24 DAS of Col-0 plants expressing *ProUBQ10:LUC2o*
 797 growing in water deficient conditions (left) and control (right). Plants were sown under
 798 control conditions and water deficit treatment started 11 DAS.

799 **Supplementary Material**



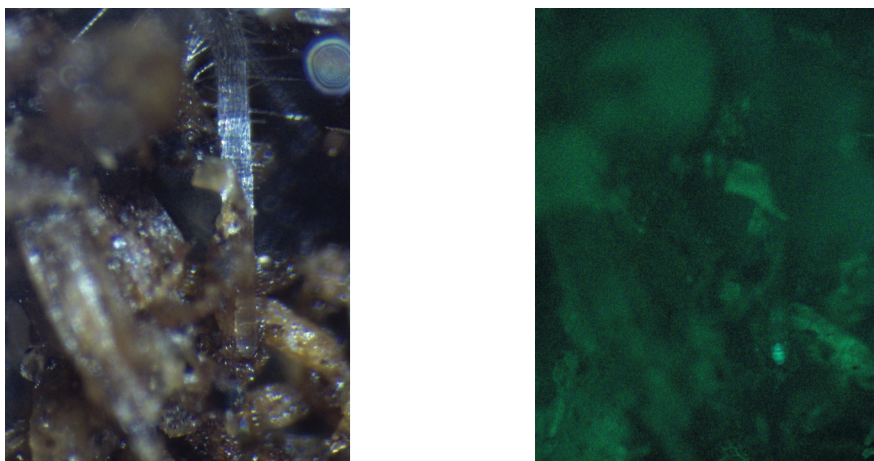
800 **Figure 1-figure supplement 1** A) Principal Components Analysis (PCA) score plot of
 801 a set of 77 genes analyzed by qPCR from root samples of plants grown in MS plates, pots,
 802 and rhizotrons. After 15 DAS three plants were collected at the end of the day (D) and
 803 three were collected at the end of the night (N). (ms = plant grown in full ms, ms25 =
 804 plants grown in 25% of full ms) B) Lateral root number and G) primary root length of 18
 805 806 807 808 DAS plants grown in 30 cm tall cylinders, pots and rhizotrons, all with a volume of 100 cm^3
 (n = 6-12 plants). D) Leaf area and E) primary root length of plants of the same age (15
 809 810 811 812 DAS) as the ones used for the qPCR experiment (n= 6-7). ANOVA analysis with p < 0.01

809 was used to test significant differences between the different parameters.

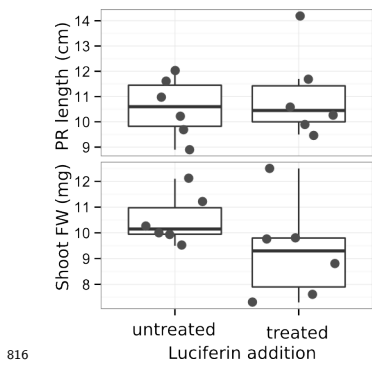


810 811 **Figure 1-figure supplement 2** PCA plot of shoots of the same samples used in Figure 1.

812 See Figure 1 for more details regarding experimental conditions used.

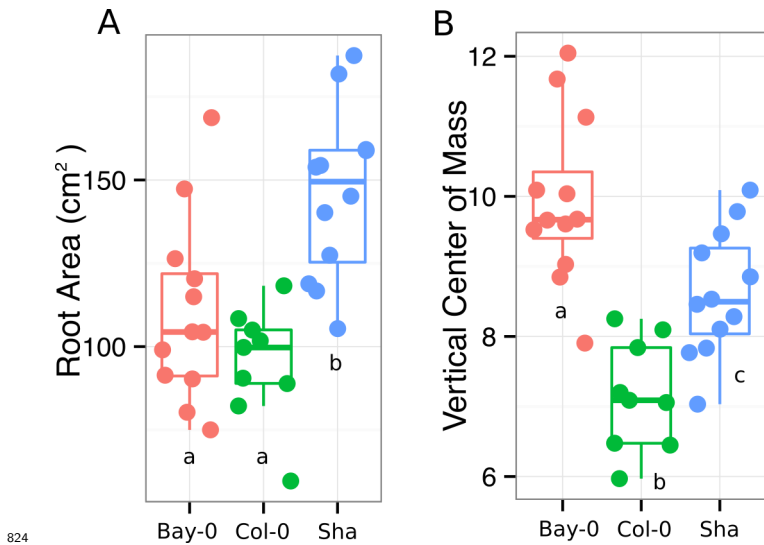


813 **Brightfield** 814 **GFP**
815 **Figure 1-figure supplement 3** Image of a an Arabidopsis root in soil under with white
light (brightfield) and GFP excitation light.

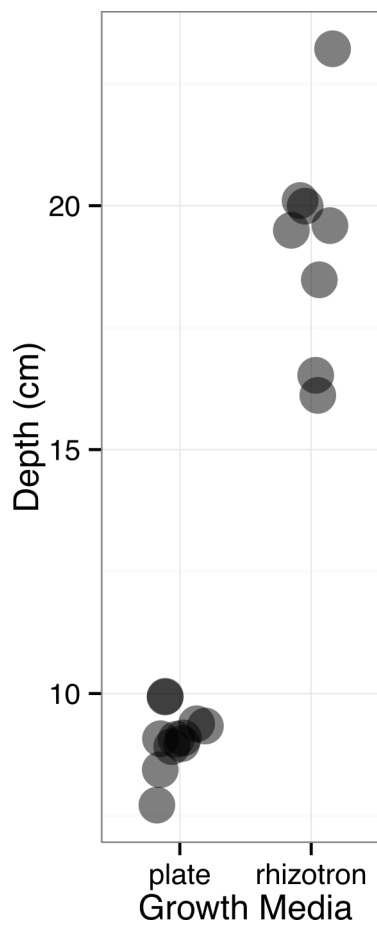


816 **Figure 1-figure supplement 4** Effect of luciferin addition on the primary root length and
 817 shoot size of 14 DAS seedlings that were either continuously exposed to 300 μ M luciferin
 818 from 9 DAS after sowing or not.
 819

820 **Figure 1-figure supplement_data_1:** Two way ANOVA P-values comparing plants
 821 grown in MS media vs plants grown in soil (pots or rhizotrons) and plants collected at day
 822 or night. We used p-value < 0.000065 threshold based on Bonferroni adjustment for multiple
 823 testing.

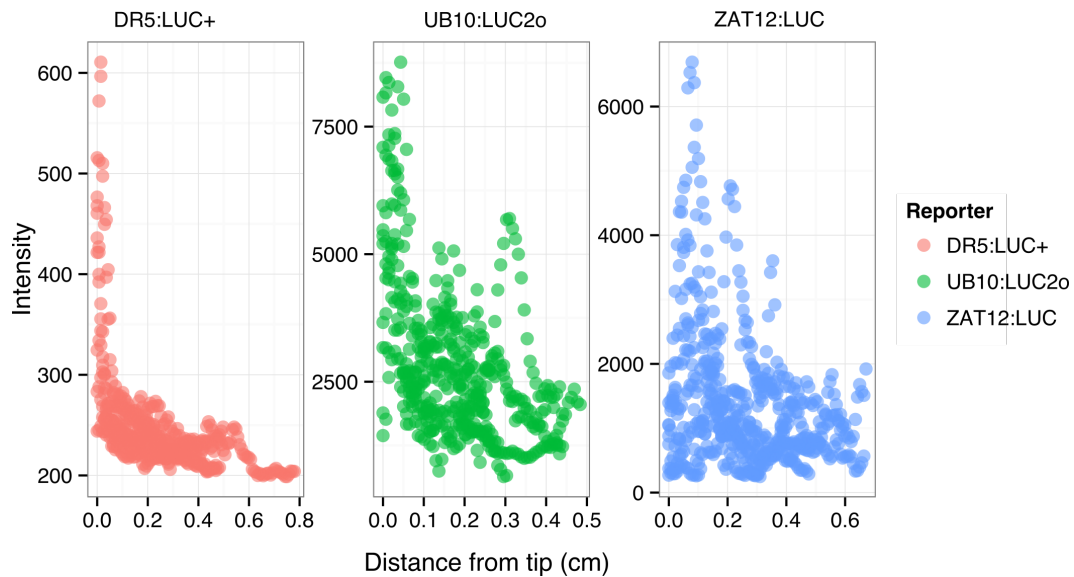


824 **Figure 3-figure supplement 1** A) root area, B) vertical center of mass of Bay-0, Col-0
 825 and Sha accessions.
 826



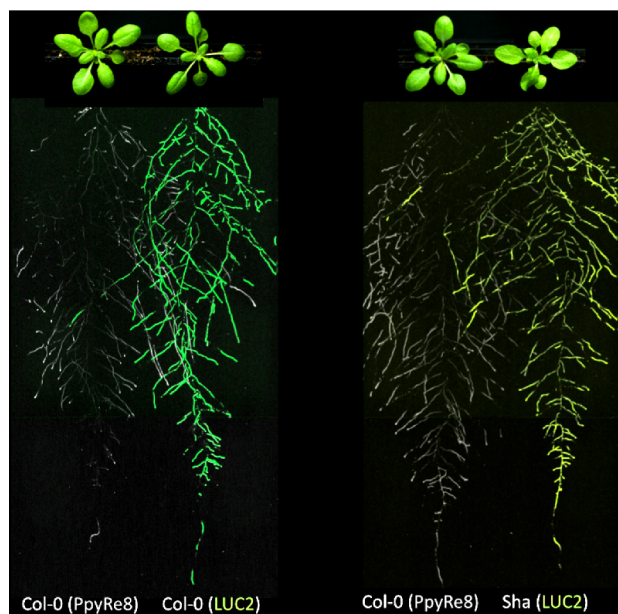
827

828 **Figure 4-figure supplement 1** Depth of the primary root of *Brachypodium* plants grown
829 in rhizotrons or on gel-based media (n=8-11).

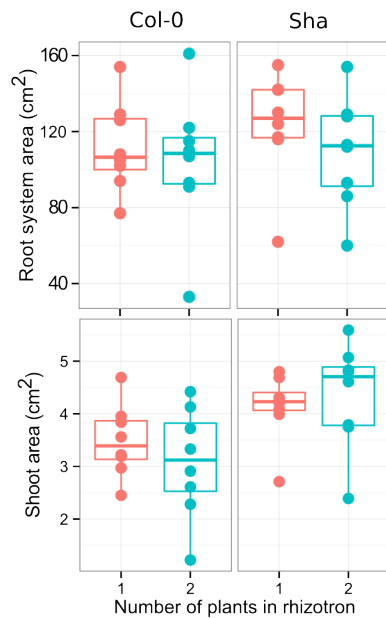


830

831 **Figure 5-figure supplement 1** Dual color images of 22 DAS plants growing in the
 832 same rhizotron and expressing different luciferases. A) Two Col-0 plants expressing
 833 *ProUBQ10:LUC2o* and *ProACT2:PPyRE8o* B) Col-0 plant expressing *ProACT2:PPyRE8o*
 834 and Sha plant expressing *ProUBQ10:LUC2o*.

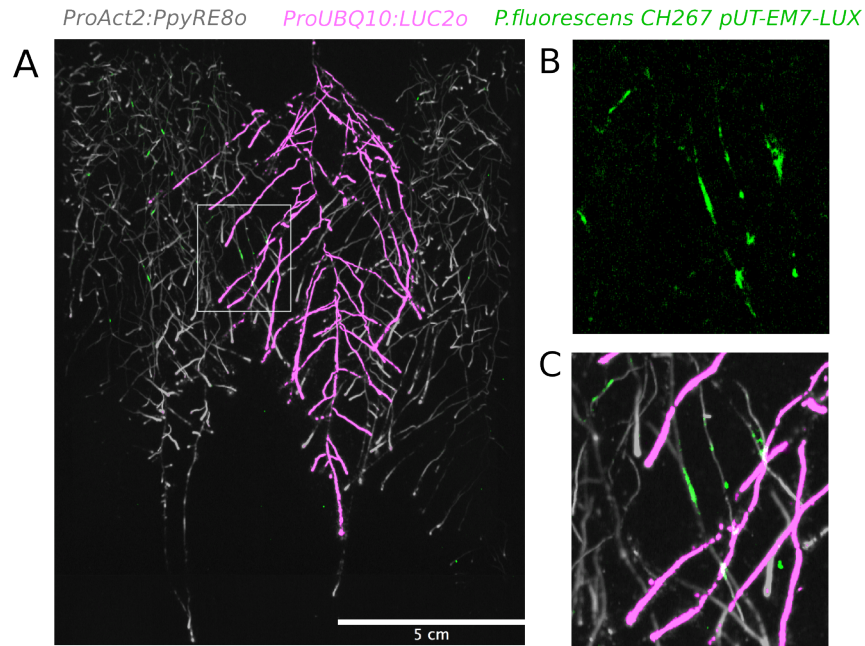


835



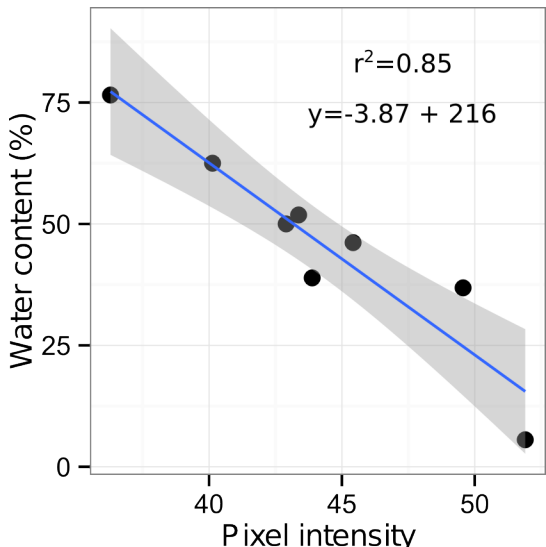
836 **Figure 5-figure supplement 2:** A) Triple color picture showing a 22 DAS
 837 *ProUBQ10:LUC2o* plant (magenta) grown in the same rhizotron with *ProACT2:PPyRE8o*

838 plants (grey). Plants were inoculated with *Pseudomonas fluorescens* CH267 (green)
839 Magnified portion of root systems colonized by *Pseudomonas fluorescens* showing *P.*
840 *fluorescences* (B) only or all three reporters together (C).



841 **Figure 5-figure**

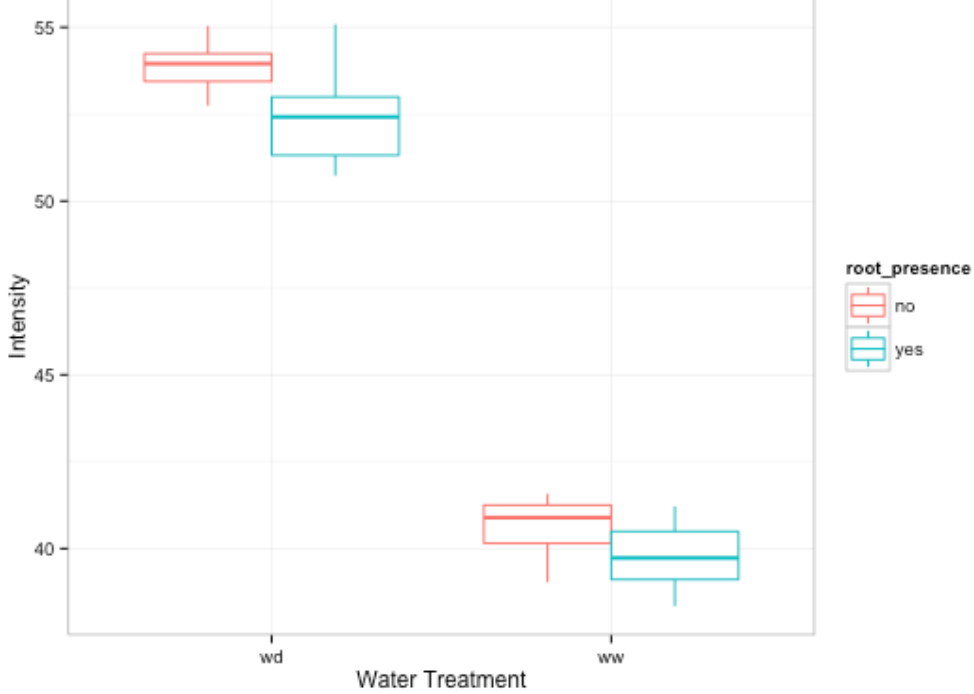
842 **supplement 3:** DR5:LUC+, UBQ10:LUC2o and ZAT12:LUC intensity values along the
843 root tip. Data was manually obtained by obtaining the intensity profile of the first 0.3-0.8
844 cm from the root tip of individual lateral roots. Ten lateral roots for each reporter were
845 measured.



846

calibration curve. Rhizotrons with different levels of moisture were prepared and scanned
847 to obtain readings of pixel intensity. Soil from rhizotrons was then weighed, dried down in
848 an oven at 70 °C for 48 hours and percent water content quantified.
849

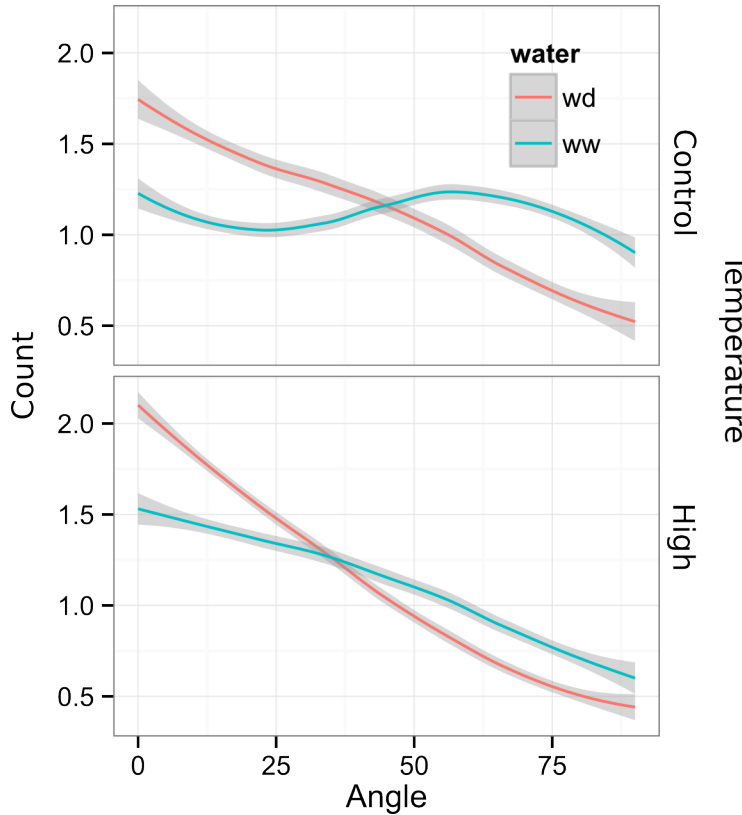
Figure 6-figure supplement 1: Moisture



850

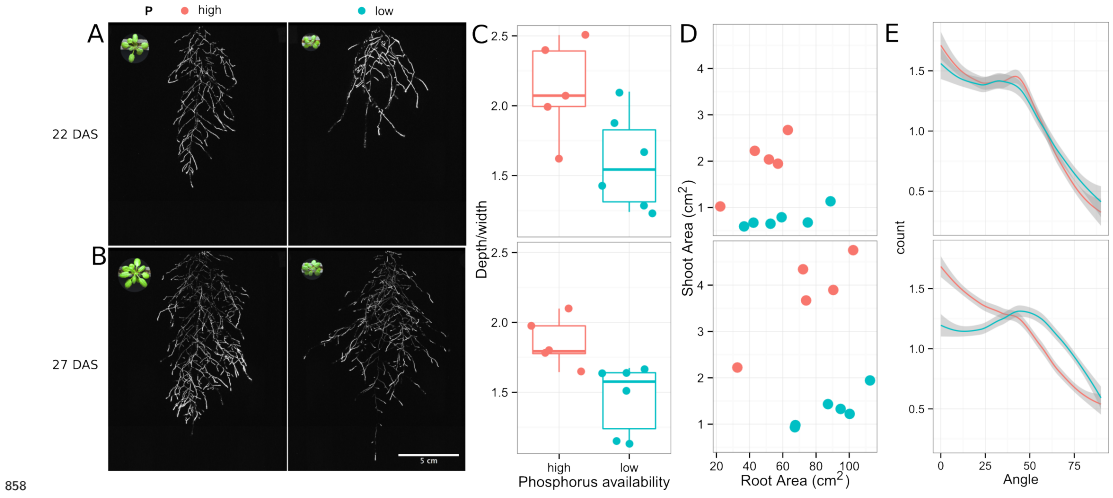
Figure 6-figure supplement 2: Comparison of soil intensity values between areas of the

852 rhizotron with or without root presence. Mean intensity values from 100 x 100 pixel squares
853 samples of both areas were obtained from 10 different rhizotrons.

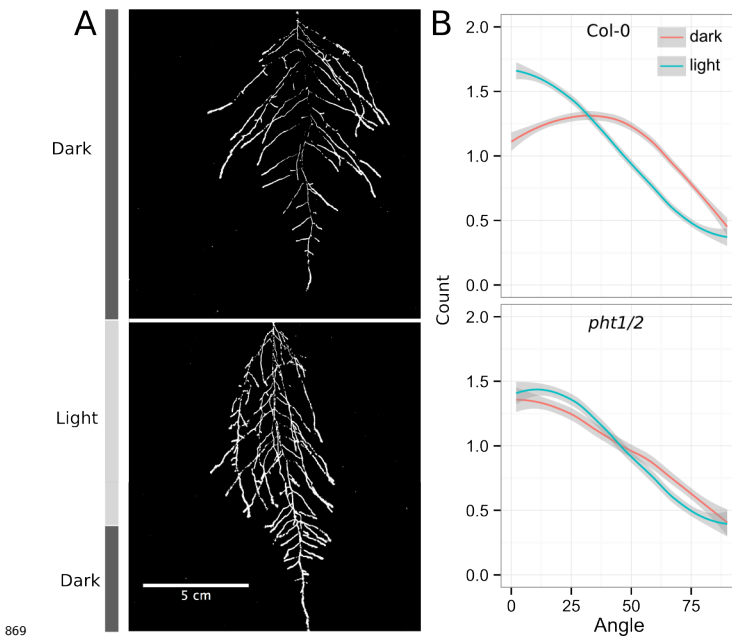


854

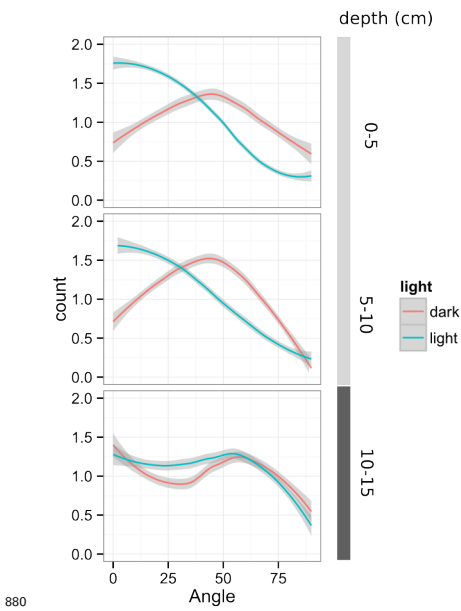
855 **Figure 7-figure supplement 1** Directionality analysis of roots of plants transferred to
856 water deprivation conditions after 9 DAS and kept 22 °C (control temperature) and 29 °C
857 (high temperature) until 22 DAS. (0° is the direction of the gravity vector).



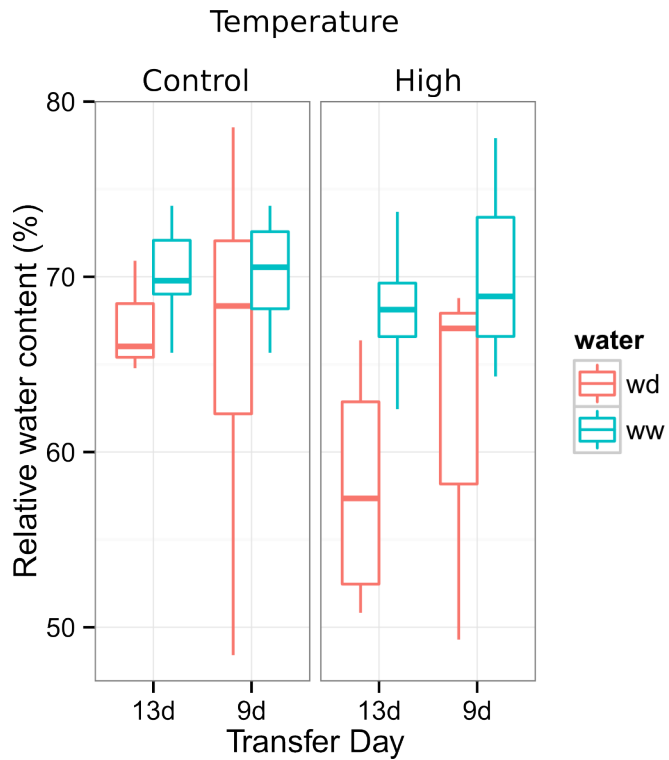
858 **Figure 7-figure supplement 2** Shoot and root systems of *ProUBQ10:LUC2o* Col-0
 859 plants growing in soil supplemented with 1ml of 100 μM P-Alumina (left) and 0-P-Alumina
 860 (right) 22 (A) or 27 (B) DAS. C) Root depth/width ratio of 22 (top) and 27 (bottom)
 861 DAS plants. D) Scatter-plot showing relationship between root and shoot system area at
 862 22 (top) and 27 (bottom) DAS. E) Root directionality distribution in plants 22 (top) and
 863 27 (bottom) DAS. Anova analysis at $p < 0.01$ was used to compare depth/width ratios in
 864 P treatments. Kolmogorov-Smirnov test at $p < 0.001$ was used to compare directionality
 865 distributions between the different treatments. A Local Polynomial Regression Fitting
 866 with 95% confidence interval (grey) was used to represent the directionality distribution
 867 curve. (0° is the direction of the gravity vector).



869 **Figure 7-figure supplement 3** A) Col-0 root systems shielded (top) or light exposed
 870 (bottom). After 9 DAS the top third of the rhizotron was exposed to light (indicated
 871 on the side with a light grey bar) and plants were imaged at 20 DAS. B) Directionality
 872 analysis of root systems shielded (red) or exposed (green) to light for Col-0 (top panel)
 873 or *pht1/2* double mutant (bottom panel). Between 4 and 6 plants were analyzed per
 874 treatment. ANOVA analysis at $p < 0.01$ was used to compare depth/width ratios in P
 875 treatments. Kolmogorov-Smirnov test at $p < 0.001$ was used to compare directionality
 876 distributions between the different treatments. A Local Polynomial Regression Fitting with
 877 95% confidence interval (grey) was used to represent the directionality distribution curve. (0°
 878 is the direction of the gravity vector).



880 **Figure 7-figure supplement 4** Plots showing output of directionality analysis performed
 881 at different depths (0-5, 5-10, 10-15 cm) in rhizotrons exposed to light or kept in the dark.
 882 (0° is the direction of the gravity vector).



884

885 **Figure 7-figure supplement 5** Leaf relative water content of 23 DAS plants that were
886 subjected to water deprivation (ww) after 9 or 13 DAS or kept under well watered (ww)
887 conditions. At 9 DAS half of the plants were kept under control temperature conditions (22
888 °C) and the other half transferred to a 29 °C (high) chamber. n = 6-8 plants.

889 **Supplemental Material 1**

890 Blueprints of the holders, clear sheets and spacers needed to built the rhizotrons. Additional
891 details are provided in the materials and methods. Files are provided in Adobe Illustrator
892 .ai and Autocad .dxf formats.

893 **Supplemental Material 2**

894 Primers used in the qPCR experiment.

895 **Supplemental Material 3**

896 Vector maps of all the constructs used in this work.

897 **References**

- 898 1.Dinneny, J. R. *et al.* Cell identity mediates the response of *Arabidopsis* roots to abiotic
899 stress. *Science* **320**, 942–945 (2008).
- 900 2.Duan, L. *et al.* Endodermal ABA Signaling Promotes Lateral Root Quiescence during
901 Salt Stress in Arabidopsis Seedlings. *Plant Cell* **25**, 324–341 (2013).
- 902 3.Lynch, J. P. & Wojciechowski, T. Opportunities and challenges in the subsoil: pathways
903 to deeper rooted crops. *J. Exp. Bot.* **66**, 2199–2210 (2015).
- 904 4.Brady, N. C. & Weil, R. R. *Elements of the nature and properties of soils*. (Prentice Hall,
905 2009).
- 906 5.Bao, Y. *et al.* Plant roots use a patterning mechanism to position lateral root branches
907 toward available water. *Proc Natl Acad Sci* **111**, 9319–9324 (2014).
- 908 6.Tabata, R. *et al.* Perception of root-derived peptides by shoot LRR-RKs mediates systemic
909 N-demand signaling. *Science* **346**, 343–346 (2014).

- 910 7.Rosquete, M. R. *et al.* An Auxin Transport Mechanism Restricts Positive Orthogravit-
911 ropism in Lateral Roots. *Current Biology* **23**, 817–822 (2013).
- 912 8.Uga, Y. *et al.* Control of root system architecture by DEEPER ROOTING 1 increases
913 rice yield under drought conditions. *Nat. Genet.* **45**, 1097–1102 (2013).
- 914 9.Postma, J. A. & Lynch, J. P. The optimal lateral root branching density for maize depends
915 on nitrogen and phosphorus availability. *Plant Physiol.* **166**, 590–602 (2014).
- 916 10.Schneider, C. A., Rasband, W. S. & Eliceiri, K. W. NIH Image to ImageJ: 25 years of
917 image analysis. *Nature methods* **9**, 671–675 (2012).
- 918 11.Hara-Miyauchi, C. *et al.* Bioluminescent system for dynamic imaging of cell and animal
919 behavior. *Biochem. Biophys. Res. Commun.* **419**, 188–193 (2012).
- 920 12.Emami, S., Yee, M.-C. & Dinneny, J. R. A robust family of Golden Gate Agrobacterium
921 vectors for plant synthetic biology. *Front. Plant Sc.* **4**, 339 (2013).
- 922 13.Ristova, D. *et al.* RootScape: a landmark-based system for rapid screening of root
923 architecture in Arabidopsis. *Plant Physiology* **161**, 1086–1096 (2013).
- 924 14.Lobet, G. *et al.* Root System Markup Language: toward a unified root architecture
925 description language. *Plant Physiol.* **167**, 617–627 (2015).
- 926 15.Meijon, M., Satbhai, S. B., Tsuchimatsu, T. & Busch, W. Genome-wide association study
927 using cellular traits identifies a new regulator of root development in. *Nat. Genet.* **46**, 77–81
928 (2013).
- 929 16.Pacheco-Villalobos, D. & Hardtke, C. S. Natural genetic variation of root system archi-
930 tecture from Arabidopsis to Brachypodium: towards adaptive value. *Philosophical Trans-
931 actions of the Royal Society of London B: Biological Sciences* **367**, 1552–1558 (2012).
- 932 17.Watt, M., Schneebeli, K., Dong, P. & Wilson, I. W. The shoot and root growth of
933 Brachypodium and its potential as a model for wheat and other cereal crops. *Functional
934 Plant Biol.* **36**, 960–969 (2009).
- 935 18.Mann, D. G. J. *et al.* Gateway-compatible vectors for high-throughput gene functional

- 936 analysis in switchgrass (*Panicum virgatum* L.) and other monocot species. *Plant Biotechnol.*
937 *J.* **10**, 226–236 (2012).
- 938 19.Pacheco-Villalobos, D., Sankar, M., Ljung, K. & Hardtke, C. S. Disturbed Local
939 Auxin Homeostasis Enhances Cellular Anisotropy and Reveals Alternative Wiring of
940 Auxin-ethylene Crosstalk in *Brachypodium distachyon* Seminal Roots. *PLoS Genet* **9**,
941 e1003564 (2013).
- 942 20.Buer, C. S., Wasteneys, G. O. & Masle, J. Ethylene modulates root-wave responses in
943 *Arabidopsis*. *Plant Physiology* **132**, 1085–1096 (2003).
- 944 21.Moreno-Risueno, M. A. *et al.* Oscillating gene expression determines competence for
945 periodic *Arabidopsis* root branching. *Science* **329**, 1306–1311 (2010).
- 946 22.Miller, G. *et al.* The plant NADPH oxidase RBOHD mediates rapid systemic signaling
947 in response to diverse stimuli. *Science Signaling* **2**, ra45 (2009).
- 948 23.Haney, C. H., Samuel, B. S., Bush, J. & Ausubel, F. M. Associations with rhizo-
949 sphere bacteria can confer an adaptive advantage to plants. *Nature Plants* 15051 (2015).
950 doi:[10.1038/nplants.2015.51](https://doi.org/10.1038/nplants.2015.51)
- 951 24.Mandoli, D. F., FORD, G. A., WALDRON, L. J., NEMSON, J. A. & Briggs, W. R. Some
952 spectral properties of several soil types: implications for photomorphogenesis*. *Plant Cell*
953 *Environ.* **13**, 287–294 (1990).
- 954 25.Galen, C., Rabenold, J. J. & Liscum, E. Functional ecology of a blue light photoreceptor:
955 effects of phototropin-1 on root growth enhance drought tolerance in *Arabidopsis thaliana*.
956 *New Phytol.* **173**, 91–99 (2007).
- 957 26.Moni, A., Lee, A. Y., Briggs, W. R. & Han, I. S. The blue light receptor Phototropin 1
958 suppresses lateral root growth by controlling cell elongation. *Plant Biology* 34–40 (2014).
- 959 27.Yokawa, K., Kagenishi, T. & Baluška, F. Root photomorphogenesis in laboratory-
960 maintained *Arabidopsis* seedlings. *Trends Plant Sci.* **18**, 117–119 (2013).
- 961 28.Lobell, D. B. *et al.* Greater Sensitivity to Drought Accompanies Maize Yield Increase in

- 962 the U.S. Midwest. *Science* **344**, 516–519 (2014).
- 963 29.Ort, D. R. & Long, S. P. Limits on Yields in the Corn Belt. *Science* **344**, 484–485 (2014).
- 964 30.Blossfeld, S., Schreiber, C. M., Liebsch, G., Kuhn, A. J. & Hinsinger, P. Quantitative
965 imaging of rhizosphere pH and CO₂ dynamics with planar optodes. *Annals of Botany* **112**,
966 267–276 (2013).
- 967 31.Shaw, S. L. & Ehrhardt, D. W. Smaller, Faster, Brighter: Advances in Optical Imaging
968 of Living Plant Cells. *Annu. Rev. Plant Biol.* **64**, 351–375 (2013).
- 969 32.Barr, H. & Weatherley, P. A re-examination of the relative turgidity technique for esti-
970 mating water deficit in leaves. *Aust. J. Biol. Sci* **15**, 413–428 (1962).
- 971 33.Grapov, D. DeviumWeb: Dynamic Multivariate Data Analysis and Visualization Plat-
972 form.
- 973 34.Branchini, B. R. *et al.* Red-emitting luciferases for bioluminescence reporter and imaging
974 applications. *Analytical Biochemistry* **396**, 290–297 (2010).
- 975 35.Branchini, B. R. *et al.* Thermostable red and green light-producing firefly luciferase
976 mutants for bioluminescent reporter applications. *Analytical Biochemistry* **361**, 253–262
977 (2007).
- 978 36.Hall, M. P. *et al.* Engineered Luciferase Reporter from a Deep Sea Shrimp Utilizing a
979 Novel Imidazopyrazinone Substrate. *ACS Chem. Biol.* **7**, 1848–1857 (2012).
- 980 37.Lane, M. C., Alteri, C. J., Smith, S. N. & Mobley, H. L. T. Expression of flagella is
981 coincident with uropathogenic Escherichia coli ascension to the upper urinary tract. *Proc.
982 Natl. Acad. Sci. U.S.A.* **104**, 16669–16674 (2007).
- 983 38.Ruegger, M. *et al.* The TIR1 protein of Arabidopsis functions in auxin response and is
984 related to human SKP2 and yeast grr1p. *Genes Dev* **12**, 198–207 (1998).
- 985 39.Moriwaki, T. *et al.* Hormonal Regulation of Lateral Root Development in Arabidopsis
986 Modulated by MIZ1 and Requirement of GNOM Activity for MIZ1 Function. *Plant Physiol.*
987 **157**, 1209–1220 (2011).

- 988 40.Vogel, J. & Hill, T. High-efficiency Agrobacterium-mediated transformation of Brachy-
989 podium distachyon inbred line Bd21-3. *Plant Cell Rep* **27**, 471–478 (2008).
- 990 41.Covington, M. F. & Harmer, S. L. The Circadian Clock Regulates Auxin Signaling and
991 Responses in Arabidopsis. *Plos Biol* **5**, e222 (2007).
- 992 42.Lindeboom, J. J. *et al.* A Mechanism for Reorientation of Cortical Microtubule Arrays
993 Driven by Microtubule Severing. *Science* **342**, 1245533–1–1245533–11 (2013).
- 994 43.Chitwood, D. H. *et al.* A modern ampelography: a genetic basis for leaf shape and
995 venation patterning in grape. *Plant Physiology* **164**, 259–272 (2014).
- 996 44.Iwata, H. & Ukai, Y. SHAPE: a computer program package for quantitative evaluation of
997 biological shapes based on elliptic Fourier descriptors. *The Journal of heredity* **93**, 384–385
998 (2002).
- 999 45.R Core Team. *R: A language and environment for statistical computing*. (R Foundation
1000 for Statistical Computing, 2014). at <<http://www.R-project.org/>>
- 1001 46.Wickham, H. *Tidyr: Easily tidy data with spread() and gather() functions*. (2014). at
1002 <<http://CRAN.R-project.org/package=tidyr>>
- 1003 47.Auguie, B. *GridExtra: Functions in grid graphics*. (2012). at <<http://CRAN.R-project.org/package=gridExtra>>
- 1005 48.Dryden, I. L. *Shapes: Statistical shape analysis*. (2013). at <<http://CRAN.R-project.org/package=shapes>>
- 1007 49.Adams, D. & Otarola-Castillo, E. Geomorph: An r package for the collection and analysis
1008 of geometric morphometric shape data. *Methods in Ecology and Evolution* **4**, 393–399 (2013).
- 1009 50.Wickham, H. *Ggplot2: Elegant graphics for data analysis*. (Springer New York, 2009).
1010 at <<http://had.co.nz/ggplot2/book>>